

1978

Fracture resistance of eyebars on the liberty bridge, M.S. thesis, May 1978.

Michael Francis Trznadel Jr.

Follow this and additional works at: <http://preserve.lehigh.edu/engr-civil-environmental-fritz-lab-reports>

Recommended Citation

Trznadel, Michael Francis Jr., "Fracture resistance of eyebars on the liberty bridge, M.S. thesis, May 1978." (1978). *Fritz Laboratory Reports*. Paper 492.
<http://preserve.lehigh.edu/engr-civil-environmental-fritz-lab-reports/492>

This Technical Report is brought to you for free and open access by the Civil and Environmental Engineering at Lehigh Preserve. It has been accepted for inclusion in Fritz Laboratory Reports by an authorized administrator of Lehigh Preserve. For more information, please contact preserve@lehigh.edu.

420.17

FRACTURE RESISTANCE OF
EYEBARS ON THE LIBERTY BRIDGE
by
Michael Francis Trznadel, Jr.

FRITZ ENGINEERING
LABORATORY LIBRARY

FRACTURE RESISTANCE OF
EYEBARS ON THE LIBERTY BRIDGE

420.11

by

Michael Francis Trznadel, Jr.

A Thesis

Presented to the Graduate Committee

of Lehigh University

in Candidacy for the Degree of

Master of Science

in

Civil Engineering

FRITZ ENGINEERING
LABORATORY LIBRARY

Lehigh University

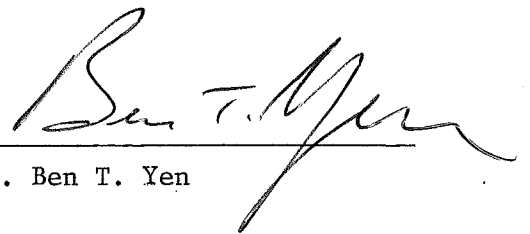
Bethlehem, Pennsylvania

May 1978

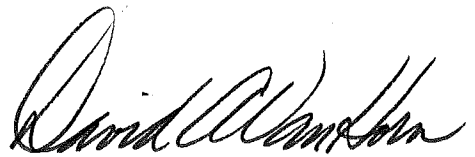
CERTIFICATE OF APPROVAL

This thesis is accepted and approved in partial fulfillment
of the requirements for the degree of Master of Science in Civil
Engineering.

May 4, 1978

A handwritten signature in cursive script, reading "Ben T. Yen", written over a horizontal line.

Dr. Ben T. Yen

A handwritten signature in cursive script, reading "David A. VanHorn", written over a horizontal line.

Dr. David A. VanHorn

ACKNOWLEDGMENTS

The research reported herein was conducted at Fritz Engineering Laboratory, Lehigh University, Bethlehem, Pennsylvania. The Director of Fritz Engineering Laboratory is Dr. Lynn S. Beedle and the Chairman of the Department of Civil Engineering is Dr. David A. VanHorn. This work is part of a study on the Fatigue and Fracture Resistance of Eyebars on the Liberty Bridge sponsored by Salvucci Associates, Inc. and the Pennsylvania Department of Transportation.

The help and guidance of Dr. J. W. Fisher, Project Director, is greatly appreciated and special thanks are due to Dr. B. T. Yen, thesis supervisor, for his untiring aid in developing this thesis.

The author also acknowledges the help of Mr. Harry Laatz and Mr. Thomas Krylowski from the Federal Highway Administration and Mr. Hugh Sutherland, Instrumentation Specialist, in acquiring the test data.

The staff of Fritz Engineering Laboratory is acknowledged for their support throughout this investigation. The insight in the finite element analysis and computer methods by Dr. S. Tumminelli is appreciated. J. M. Gera drafted the figures and special thanks to Mrs. Dorothy Fielding for her aid in typing this manuscript.

TABLE OF CONTENTS

ABSTRACT	1
1. INTRODUCTION	2
1.1 Historical Background	2
1.2 Description of the Liberty Bridge	3
1.3 Objectives and Approach	4
2. PRELIMINARY RESULTS OF FIELD STUDIES	7
2.1 Field Inspection of Eyebars	7
2.2 Live Load Stresses in Eyebars	8
2.3 Dead Load Stresses In Eyebars U 35 - U 36	10
3. STRESS DISTRIBUTION IN EYEBAR HEADS	12
3.1 Design Parameters and Assumptions	12
3.2 Finite Element Model	14
3.3 Comparison with Test Results	17
3.4 Stress Concentration Factor at Eyebars Pin Holes	19
4. FRACTURE RESISTANCE AND FATIGUE STRENGTH	21
4.1 Fracture Resistance	21
4.1.1 Approximations In Correction Factors	22
4.1.2 Stress Intensity Factor and Critical Crack Size	24
4.2 Fatigue Strength	25

TABLE OF CONTENTS (continued)

5.	DISCUSSION	29
5.1	Stress Evaluation	29
5.2	Bonded Eyebars Heads	30
5.3	Anticipated Conditions	31
6.	CONCLUSIONS AND RECOMMENDATIONS	32
	NOMENCLATURE	35
	TABLES	37
	FIGURES	39
	REFERENCES	72
	VITA	75

.....
LIST OF TABLES

Table		Page
1	MAXIMUM MEASURED STRESS RANGE IN EYEBAR SHANKS	37
2	DESIGN CRITERIA FOR PROPORTIONING EYEBAR HEADS	38

LIST OF FIGURES

<u>Figure</u>		<u>Page</u>
1	Elevation of Liberty Bridge Looking West (Downstream)	39
2	Locations of Eyebars on the Main Spans Over the River	40
3	Typical Cross Section of the Liberty Bridge	41
4	Eyebar Head U 36A with Pin Cap Removed	42
5	Sandblasted Eyebar Head Showing Forging Marks	42
6	Variation in Live Load Stress versus Time For Truck in Different Lanes	43
7	Measured Stress Ranges for Test Truck in Curb Lane, Northbound	44
8	Dimensions of Eyebars at U 35 - U 36	45
9	Typical arrangement of Strain Gages for Live Load and Dead Load Study	46
10	Non-dimensionalized Measured Stress Distribution - U 36A Dead Load	47
11	Non-dimensionalized Measured Stress Distribution - U 36A Partial Load	48
12	Non-dimensionalized Measured Stress Distribution - U 35A Dead Load	49
13	Non-dimensionalized Measured Stress Distribution - U 35A Partial Load	50

LIST OF FIGURES (continued)

<u>Figure</u>		<u>Page</u>
14	Non-dimensionalized Measured Stress Distribution - U 36D Dead Load	51
15	Non-dimensionalized Measured Stress Distribution - U 36D Partial Load	52
16	Dead Load Stresses in Shanks of Eyebars U 35 - U 36	53
17	Symbols Used to Describe Eyebars Geometry	54
18	Discretization of Eyebars Head With Curved Transition	55
19	Discretization of Eyebars Head with Straight Line Approximation	56
20	The Effect of Curved and Straight Line Transition on the Stress Distribution	57
21	Discretization and Boundary Conditions of Substructure for a Fine Mesh Analysis	58
22	Effect of Finite Element Size on Stress Distribution	59
23	Comparison of Finite Element Analysis Results and Measured Values	60
24	Results of Gross Mesh Analysis of Eyebars U 35 - U 36 on the Liberty Bridge	61
25	Comparison of Measured and Theoretical Stress Distributions for U 36A	62

LIST OF FIGURES (continued)

<u>Figure</u>		<u>Page</u>
26	Enlarged Plot of Gross and Fine Mesh Analysis Results	63
27	Stress Distribution for Eyebar Heads with Different Width Ratios, Gross Mesh	64
28	Effect of Pin Hole Size on the SCF, Gross Mesh	65
29	Effect of Shank Width on the SCF, Gross Mesh	66
30	Front Free Surface Correction Factor, F_s	67
31	Assumed Crack Shape at Edge of Pin Hole	68
32	Stress Concentration Factor K_t and Stress Gradient Correction Factor, F_g as a Function of Crack Size	69
33	Stress Intensity Factor as a Function of Crack Size	70
34	Test Results of K_{Ic} for Eyebar Material (AISI 1035 Heat-Treated Steel)	71

ABSTRACT

This study is based on the Liberty Bridge which is in Pittsburgh, Pennsylvania and crosses the Monongahela River. The bridge is being evaluated for rehabilitation and the progress to date is summarized in this report. Both field and laboratory studies were made and special attention is given to the fracture resistance and fatigue strength of the eyebars.

Field work included inspection of eyebar heads, live load and dead load stress measurements, and removal of two existing eyebars which were replaced by new ones. Material properties and stresses in the bridge members were evaluated. The distribution and magnitude of stresses in the eyebar heads were examined by a finite element procedure. The possibility of fatigue crack growth from flaws at eyebar head pin holes and the critical crack size which would cause brittle fracture were investigated.

Analysis shows the maximum stress concentration factor at the edge of the pin hole for eyebars designed by the specifications to be around 3.5. Under the existing and anticipated loads, the stresses in eyebars were found to be very low and as a result the possibility of fatigue crack growth and brittle fracture is remote. Based on these findings the planned rehabilitation of the Liberty Bridge is recommended.

1. INTRODUCTION

1.1 Historical Background

Bridges which utilize eyebars as primary tension members date back to the old Budapest Suspension Bridge, built in 1849 by W. Tierney Clark. The eyebars of this bridge are believed to be made of an iron alloy. Steel eyebars were first introduced, for the use in bridges, around the year 1880 and heat-treated carbon steel eyebars were developed in 1914^{1,2}.

With the advent of high strength wire rope and new construction methods the eyebar was not used as often in the design of bridges after the early 1930's.

The designers of eyebar bridges during the late 1800's and early 1900's did not have the benefit of considering stress corrosion cracking, corrosion fatigue, or fatigue crack growth in their analysis since these considerations were not sufficiently developed. After the recent (1967) collapse of the Point Pleasant Bridge connecting Point Pleasant, West Virginia, and Kanauga, Ohio the possibility of other eyebar bridge failures became a major concern³. The failure of this bridge cost the lives of 46 persons. The bridge was an eyebar cable suspension type and the material used for the eyebars was a heat-treated carbon steel conforming to the specifications for AISI 1060 steel. The National Transportation Safety Board Report on the

Point Pleasant Bridge³ indicates that collapse of the bridge structure was attributed to failure of an eyebar caused by stress corrosion and/or corrosion fatigue resulting in growth of a flaw to a critical size.

The failure of the Point Pleasant Bridge immediately made suspect other eyebar bridges to fatigue crack growth and brittle fracture. Most of the eyebar bridges in the United States were constructed in the early 1900's and the materials used for the eyebars were primarily heat-treated carbon steels. The Liberty Bridge is one such bridge that utilized eyebars as primary tension members and is the subject of this study.

1.2 Description of the Liberty Bridge

The Liberty Bridge is a deck type continuous truss structure as shown in Fig. 1. It has a four lane roadway which carries northbound and southbound traffic to and from Pittsburgh, Pennsylvania over the Monongahela River. The total length of the bridge is about 794 meters (2605 feet) with two main truss spans of 143.4 meters (470.5 feet) over the river. There are three short girder spans and three truss spans over the railroad tracks and streets at the south end, and two girder spans and three truss spans over the parkway, railroad and avenue at the north end.

The top chords of the trusses in the negative moment regions over the piers are tension members and utilize eyebars. (See Fig. 2) The eyebars are made of AISI 1035 heat-treated carbon steel.

The bridge has a floor beam and stringer system with a non-composite concrete deck and an asphalt wearing surface. A typical cross section of the bridge is shown in Fig. 3. Construction of the bridge was finished in 1928.

1.3 Objectives and Approach

The objective of the overall study on the Liberty Bridge is to evaluate the safety and integrity of the bridge for continued service and the planned life of the structure. The bridge is to be rehabilitated with a widened deck replacing the present deteriorated one.

The specific goal of this study, of which some preliminary results are reported herein, is to investigate the fatigue strength and fracture resistance of the eyebars. The approach to achieve this goal consists of the following steps.

1. Inspection of the eyebars, particularly the eyobar heads:-This work was carried out in the field and in the laboratory, when a couple of eyebars removed from the bridge have been examined.
2. Measurement of live load stresses:-Since a vehicular weight limit has been posted for the bridge, a special test truck was employed. Stresses in eyobar shanks and heads were monitored using electrical resistance strain gages.

3. Measurement of dead load stresses in eyebars:-Dead load stresses can only be measured by relieving the loads in eyebars. Mechanical devices and hydraulic jacks were used to accomplish this. Two eyebars were removed from the bridge for studies in the laboratory.
4. Determination of material properties of eyebars:-Of primary concern is the fracture toughness of the eyebar material. Standard specimens for evaluating this material property have been fabricated from the eyebars which were removed from the bridge.
5. Analysis and evaluation of stress distribution in eyebars and eyebar heads:-The stress distribution among eyebar groups, within each shank, and in the eyebar heads were evaluated using measured stress values. The finite element procedure was utilized to analyze stress distributions in eyebar heads with different dimensions.
6. Evaluation of fatigue strength and fracture resistance of eyebars:-The fatigue strength is estimated in terms of the nominal live load stress in eyebar shanks and the anticipated number of load cycles to failure. Failure is when a fatigue crack would have grown in size to the critical dimensions which would cause sudden brittle fracture under adverse conditions.

While work is still in progress, some preliminary results have been obtained and are summarized briefly in this report. Some preliminary conclusions are also drawn. More comprehensive conclusions and recommendations will be made when all phases of the study have been completed.

2. PRELIMINARY RESULTS OF FIELD STUDIES

2.1 Field Inspection of Eyebars

Eyebars pin caps were removed from panel points U 35, U 36 and U 47 of the upstream truss for inspection of the eyebars holes. The locations of these panel points are shown in Fig. 2. For identification purposes, eyebars in a group were arbitrarily designated A, B, C and D from upstream towards downstream. Eyebars U 35 - U 36A and D were originals whereas U 35 - U 36B and C are reinforcing eyebars which were added in 1974 to eliminate any two-eyebars panels in the bridge.

The exposed eyebars head U 36A is shown in Fig. 4. Visual inspection with a magnifying glass did not reveal any cracks or sharp notches at the eyebars heads U 35A, U 35D, U 36A, U 36D and U 47A. The Acoustic Crack Detector (ACD) of the Federal Highway Administration was also used and did not find any cracks or flaws in the same eyebars heads. The eyebars head faces, however, had forging marks which could be seen after the faces were sandblasted clean. An example is shown in Fig. 5. These forging marks were not situated at the crucial points, nor were the directions of the marks perpendicular to the primary stresses in the heads. Since the ACD could not detect their presence, the depth of these marks were assumed to be shallow. Later examinations in the laboratory did not reveal any adverse condition.

The pins and pin holes at U 35 and U 36 appeared to be in fairly good condition by visual inspection after the eyebars were removed from the panel. The holes were slightly larger than the pins and were very slightly elongated under the dead weight of the bridge. When the dead loads were removed from eyebars U 35 - U 36A and D, there was no apparent permanent deformation at the holes. There was some indication of corrosion in the pins between eyebars at these two panel points, but was quite moderate when compared to the corroded condition of some steel parts of the deck system. The eyebar shanks generally were in fairly good condition except for the existence of bird droppings. Some eyebar heads, such as U 35 and U 36, have also been subjected to excessive moisture due to the deteriorated condition of the deck. The pin caps, bolts and nuts, however, were in excellent condition.

2.2 Live Load Stresses in Eyebars

Live load stresses correspond to vehicular loads. Since the bridge was closed to any vehicle 89 kN (20 kips) or heavier, the live load stresses were expected to be small. This was confirmed in 1974 and reconfirmed during this field study in 1977. All measured stresses by passenger cars and buses were less than 3.45 MPa (0.5 ksi) in the shanks of the eyebars.

To examine the possible live load stresses in the eyebars, a test truck and snoopers from the Pennsylvania Department of Transportation, weighing approximately 351 kN (79.0 kips) and 200 kN

(45.0 kips) respectively, were driven back and forth over the bridge. The truck and the snoopers traveled alone, side by side, or in tandem. The recorded maximum stress ranges (live load stresses) at various eyebar shanks are summarized in Table 1. The highest maximum stress range was 10.0 MPa (1.45 ksi) in eyebar U 46 - U 47B and occurred when the trucks were traveling abreast near the eyebar.

The position of trucks influence the live load stress magnitude in structural elements. Traces of time variation of stresses in eyebar U34 - U 35A are presented in Fig. 6 for the situation of the test truck traveling in different lanes. Lane 1 is the north-bound curb lane adjacent to the eyebar in the upstream truss. These traces are analogous to influence lines for a load of 351 kN (79.0 kips) over a length of approximately 30 meters (98 ft.) Because the bridge has only two trusses, trucks traveling south, adjacent to the downstream truss, also generate stresses in the eye-bars of the north truss, as is evident from Fig. 6. For the evaluation of fatigue strength of the eyebars and other components, traffic in both directions must be considered.

The distribution of loads among a group of eyebars were monitored with strain gages. Figure 7 compares the live load stresses in two eyebar groups for the same truck run. Stresses were not equal in each eyebar, implying an unequal load distribution among the eyebars. Furthermore, the stresses were slightly different between the top and bottom of the eyebars. This small but noticeable difference occurred on almost all eyebars. It appears that the

eyebars were subjected to some bending such that the top of the eyebars sustained slightly higher tension.

2.3 Dead Load Stresses In Eyebars U 35 - U 36

The two original eyebars between panel points U 35 and U 36 were removed for laboratory studies and were replaced by two new eyebars of the same dimensions. The dimensions are shown in Fig. 8. Strain gages were mounted on the original eyebars as shown in Fig. 9 to monitor the change of strains during removal. During the process, hydraulic jacks transferred the dead load forces from eyebars U 35 - U 36A and D to the reinforcing bars U 35 - U 36B and C. For the purpose of strain measurement, forces were transferred back to the original bars, and then completely relieved so that the eyebars could be removed from the pins.

Difficulties were encountered in sliding the eyebars off the pins when there was apparently no load in the eyebars U 35 - U 36A and D. Upon inspection, it was found that the eyebar head faces had adhered to each other at panel points because of corrosion. The adhesive force was very strong at U 35A. Repeated lifting of U 35 - U 36A at the freed U 35A, by a hoist, could not break the adhesive bond at the other end of the eyebar. It was slid off the pin only after wedges were driven between the eyebar head faces and torches were used to burn off the corroded material.

The measured stresses in the eyebar heads confirmed the condition of adhesion between eyebar head faces. The measured stress

distribution at U 36A, as shown in Figs. 10 and 11 agrees well with that obtained by stress analysis⁴. On the other hand, the recorded stress distribution in U 35A indicated a very moderate stress gradient and is shown in Figs. 12 and 13. The magnitude of stress at the pin hole was about the same as that in the shank of the eyebar. This condition implies that the force transmitted at U 35A was not through the pin, rather it was through the bond between the faces of joining eyebars U 34 - U 35A and U 35 - U 36A in adjacent panels.

The measured stresses from the limited number of strain gages at eyebar head U 36D also revealed the same condition of force transmitted through surface bond. The stress distribution in this eyebar head is given in Figs. 14 and 15 for the same jacking force as for Figs. 10 to 13. The values presented are the stress non-dimensionalized by the average stress in the eyebar shank.

The distribution of stresses in the shanks of eyebars U 35 - U 36 are depicted in Fig. 16. During removal (unloading) of forces from eyebars U 35 - U 36A and D, stresses decreased in A and D while they increased in reinforcing bars U 35 - U 36B and C. These stresses provided an on-the-spot monitoring of the eyebar removal operation. The most important stresses were in the heads of the eyebars.

3. STRESS DISTRIBUTION IN EYEBAR HEADS

3.1 Design Parameters and Assumptions

Because maximum stresses are higher in the heads than in the shank of eyebars, and the distribution of these stresses are not uniform, it is necessary to evaluate the maximum stresses in the heads of eyebars. In the design of eyebars in the past, however, the stress distribution analysis was usually omitted when the eyebars were proportioned according to design specifications.

Table 2 lists the design criteria for eyebars set forth by the American Institute of Steel Construction⁵ (AISC), American Association of State Highway and Transportation Officials⁶ (AASHTO) and the American Railway Engineering Association⁷ (AREA) specifications. These specifications have been established based on experimental and analytical data. In all three specifications the proportioning of the head of an eyebar is determined from the required net section of the shank. The net section of the shank is determined from the allowable stress in a tension member. The resulting design is such that the average stress is higher in the shank than in the head of an eyebar.

For the evaluation of fatigue strength and fracture resistance, the maximum stress in the head must be considered. The maximum stress could be at the circumference of the pin hole on a transverse diameter, or at the edge of the eyebar at the transition

from the shank to the head. The magnitude of this stress depends on the relative dimensions such as the width ratio and the diameter of the head, as listed in Table 2. The symbols are shown in Fig. 17.

There have been many different analytical methods of determining the stress distribution in tension members with eye-shaped heads. In this study the finite element method was chosen for its versatility and reliability of results in determining stress distributions in solid continuum.

One of the most crucial assumptions in modeling eyebars is the distribution of bearing pressure between the pin and pin hole. Blumenfeld⁸ distributed the load uniformly over the interface at the top half of the ring while Beke⁹ assumed the bearing pressure to be proportional to the cosine of the angle measured from the longitudinal axis. Reissner and Strauch¹⁰ also used a cosine distribution but included a shear stress as an external reaction caused by friction. Timoshenko and Goodier¹¹ used a cosine function but made refinements in the stress function to satisfy the compatibility relations. Poletto⁴ achieved very good correlation between a finite element analysis and test data by assuming a non-uniform cosine bearing pressure varying from the vertical to horizontal sections on the top half of the pin hole. Fisher and Daniels¹² modeled the bearing of a pin-plate on a pin by connecting radial and tangential supports to nodes at the pin surface in a finite element analysis. A more complete coverage and bibliography can be found in Ref. 4.

The method of modeling the pin with elastic supports in the radial and tangential directions was adapted for this study. The radial and tangential stiffness of the elastic supports were taken as¹²:

$$K_r = A E/d$$

$$K_t = 0.3 K_r$$

where:

K_r = radial stiffness

K_t = tangential stiffness

A = bearing area between pin and pin hole

d = pin diameter

E = modulus of elasticity.

The tangential supports simulate the effects of friction between the pin and pin hole interface. Results from trial analysis showed that the elastic supports should be spread over a 90° angle, 45° to each side of the longitudinal axis, on the top side of the pin hole.

3.2 Finite Element Model

The finite element program used in this study was SAP IV, a structural analysis program for static and dynamic response of linear elastic systems¹³.

By taking advantage of the symmetry of the eyebar about its major axis, only one-half of an eyebar head was discretized with appropriate boundary conditions along the centerline. Plane stress finite elements were used.

Because the influences of eyebar geometry on the stress distribution in eyebar heads were to be examined, large amounts of input data were required for the computer program even when plane stress elements were adapted. In view of this, stress distributions in eyebar heads were examined for possible simplification in input data. It was found that for eyebar geometry similar to that of Liberty Bridge eyebars, the maximum stress in the heads was at the pin holes, not at the transition from the shank to the head. Consequently, the curved transition from eyebar head to eyebar shank was approximated by a straight line. Figure 18 shows the discretization of the model with the curved transition and Fig. 19 shows that with the straight line approximation. This modification enabled the formulation of a computer program which would provide stress distribution output for different geometry with only slight changes in input data.

For two eyebar heads of the same loading conditions and geometry, except the transition curve, the results from the finite element analysis are given in Fig. 20. In the figure the stress distributions along a transverse diameter at the pin hole are compared. The ordinates are the stresses non-dimensionalized by the shank stress. The abscissa is the distance from the edge of the pin hole. This plot demonstrates that the effect of the straight line approximation is very small and its use has been incorporated into this investigation.

The finite element model of Fig. 19 gives the location of the maximum stress and stress distribution in a eyebar head. From the experience of the failure of the Point Pleasant Bridge³ and from results of other investigations^{14,15}, it can be concluded that, if a crack would develop, it would originate at the location of the maximum stress. The crack would then propagate along a path perpendicular to the maximum principle tensile stress in the eyebar head. This path coincides with the transverse diameter of the head.

For a fracture analysis of eyebar heads with a high stress gradient along the most probable crack path, an estimate of stresses more accurate than those given by the model in Fig. 19 is necessary. The cross hatched area of the discretization shown in the figure was used as the substructure in a fine mesh analysis. The discretization and boundary conditions for this fine mesh substructure is sketched in Fig. 21. The size of the smallest elements was 2.29 mm (0.09 in.). Plane stress elements were again used so as to conform with the overall gross mesh structure model. From the gross mesh analysis the stresses were taken along the perimeter of the substructure and converted to equivalent forces. These forces were then applied to the respective nodes at the boundary of the fine mesh substructure.

The computed stress distributions from the gross mesh and fine mesh analyses are presented in Fig. 22 for an eyebar of the Liberty Bridge. The fine mesh model gives higher maximum stress at the edge of the pin hole. Obviously, further decrease in mesh size

would result in higher stress at the point and a steeper stress gradient along the transverse diameter (the abscissa) until the "true" magnitude is reached. Results from fracture resistance analysis (Chapter 4) indicated that the chosen mesh size was adequate and thus considered sufficiently accurate.

3.3 Comparison with Test Results

To examine the validity of the finite element model used in this study, a comparison was made between the computed stresses and measured test data of Poletto⁴ on a full size eyebar from the collapsed Point Pleasant Bridge³. The eyebar tested was gaged extensively on the head to determine the stress distribution. Figure 23 shows in non-dimensionalized ordinates the distribution of stresses across the width, a , of the eyebar head on the transverse diameter. The measured results and the finite element solution values agree very well except near the outside edge of the head, where the theoretical stresses are in compression. At the pin hole, the maximum computed stress is higher than that from measurement at the specific load of Fig. 23. However, at other load magnitudes during testing, the non-dimensionalized stress (or the stress concentration factor) at the pin hole varied from 2.27 to 3.15⁴. This range is also indicated in the figure on the ordinate. This condition points out the difficulty of actual stress measurement at the pin hole, even under controlled conditions in a laboratory.

For the Liberty Bridge stress distribution in the heads of eyebars U 35 - U 36 were computed. The stresses along the transverse diameter through the pin hole and along the eyebar axis in the eyebar head are plotted in Fig. 24. Nominal dimensions of the eyebars were used with the finite element discretization model of Fig. 19. The computed stress distribution as shown in Fig. 24 confirms those obtained from measurements at eyebar head U 36A after the breaking of bonds (Figs. 10 and 11). A direct superposition is given in Fig. 25. The excellent agreement between computed and measured stresses is evident.

Higher stresses at pin holes resulted from computation when the fine mesh substructure (Fig. 21) was used. The comparison of stresses along the transverse diameter of the pin hole of U 35 - U 36 is given in Fig. 22 for the overall model and the fine mesh substructure. An enlarged plot is given in Fig. 26. The stress concentration factor from the substructuring model is 3.47 at the edge of the pin hole. It was, however, impossible to measure stress at this point due to the physical width of the electrical resistance strain gage. Judged by the excellent agreement between computed and measured stresses over the entire eyebar head, it is considered that the finite element model is adequate for analyzing stress distributions in eyebar heads.

3.4 Stress Concentration Factor at Eyebar Pin Holes

Because the most likely crack path is along the transverse diameter of a pin hole, the maximum stress at the edge of the pin hole on this diameter is most important. The magnitude of this stress is a function of the average stress in the shank of the eyebar and the geometry of the eyebar head. By using the finite element model, stresses for different geometries can be calculated.

Figure 27 depicts the stress distribution from the pin hole to the outside edge for two eyebar heads. The pin hole diameter (d) is arbitrarily taken as $7/8$ times the width of the shank (b), and the width (a) of the rim of the eyebar head is $0.665b$ and $0.75b$ respectively. These are the specified limits as summarized in Table 2. Other dimensions being the same, the head with a wider width (a) or a higher value of width ratio (a/b) has lower stresses. The pattern of stress distribution is identical and is also the same as those shown in Figs. 10 and 24 for the Liberty Bridge.

Because the width ratio (a/b) affects the stress magnitude, its influence on the stress concentration factor (SCF) at the pin hole is examined. Figure 28 shows the variation of SCF with a/b for two eyebars of different pin hole sizes (d), but the same width (b). Figure 29 shows the change of SCF with a/b for two different eyebar widths (b) but the same pin hole size (d). For all cases the width ratio a/b is the dominant controlling parameter. The SCF decreases with higher values of a/b .

The stress concentration factors in Figs. 28 and 29 were computed using a gross mesh finite element model. More accurate values can be obtained from a fine mesh analysis or substructuring technique. Coupled with the practical limits of geometry (Table 2) some guidelines could be established for eyebar design.

4. FRACTURE RESISTANCE AND FATIGUE STRENGTH

4.1 Fracture Resistance

Under an adverse combination of unfavorable conditions, sudden fracture of an eyebar or structural member may occur. The controlling factors include the stress magnitude, material properties, and flaw size, among others. In cases of structural member failure which were studied, often small flaws were found to grow, as fatigue cracks, to a critical size and triggered fracture^{12,16}. The concepts of linear elastic fracture mechanics have been used successfully in the evaluation of these failures.

The fracture resistance of an eyebar is associated with the stress intensity factor, K ^{17,18}. This factor can be expressed as

$$F = F_s \times F_w \times F_e \times F_g \times \sigma \times \sqrt{\pi a} \quad (4.1)$$

where

F_s = front free surface correction

F_w = finite width connection

F_e = crack shape correction

F_g = stress gradient correction

σ = nominal stress in the shank

a = flaw size

When the stress intensity factor with a flaw or crack in a structural detail is higher than the fracture toughness property of the material fracture will occur.

Equation 4.1 is an approximation of more exact expressions. It renders a possible simplified solution with reasonable accuracy through approximation of the individual correction factors.

4.1.1 Approximations In Correction Factors

The front free surface correction factor, F_s , accounts for the effects due to a free surface at the crack origin. The most likely position of crack initiation, in an eyebar head, is at the edge of the pin hole. Figure 30 shows the front free surface correction factors for an edge crack in a semi-infinite plate under uniform tension and under tension which varies linearly from the crack origin to the crack tip¹⁹. As the stress distribution for the eyebar lies between these two cases, a value of 1.15 was used for F_s as suggested by Tada and Irwin²⁰.

The finite width or back free surface correction, F_w , amplifies the stress intensity factor as the crack approaches a back free surface. Zettlemoyer¹⁴ suggested that if the displacements normal to the back free surface are zero the finite width correction factor can be computed by:

$$F_w = \sqrt{\frac{2w}{\pi a} \tan \frac{\pi a}{2w}} \quad (4.2)$$

If, on the other hand, the stresses are zero normal to the back free surface then¹⁴:

$$F_w = \sqrt{\sec \frac{\pi a}{2w}} \quad (4.3)$$

In both equations 4.2 and 4.3 a is the crack length and w is the width of the structural member or detail. Equation 4.2 is adopted in this investigation.

There has been little study to date on the crack shape variation in eyebar heads. An upper bound and a lower bound are assumed here for the crack shape correction factor, F_e . The lower bound corresponds to a circular corner crack as shown in Fig. 31a. The upper bound is derived from a through-the-thickness crack as shown in Fig. 31b. The corner crack is more realistic since corrosion cracks are more likely to initiate at the edge of a pin hole on the eyebar head surface where a corrosive environment would attack first. In the Point Pleasant Bridge investigation³ elliptical surface corrosion flaws at the pin hole were found on the fractured surface of the eyebar. This condition was between the lower and upper bound assumed here.

The stress gradient correction factor, F_g , accounts for the effects of non-uniform stress fields acting on the assumed crack path. Albrecht²¹ developed a formula for the stress gradient correction factor for cases where the stress concentration decay is known for discrete points from analysis.

$$F_g = \frac{2}{\pi} \sum_{j=1}^m Kt_j \left[\sin^{-1} \left(\frac{y_j + 1}{a} \right) - \sin^{-1} \left(\frac{y_j}{a} \right) \right] \quad (4.4)$$

where Kt_j is the average stress concentration over the interval from y_j to y_{j+1} , a is the crack length and y is the distance from the crack origin to a point on the crack surface²¹.

Figure 32 shows a plot of stress concentration factor, Kt , and the associate stress gradient correction factor, F_g , as a function of crack size. The stress gradient correction factor, F_g , decreases at a slower rate than does the stress concentration factor, Kt , as the crack grows in size.

4.1.2 Stress Intensity Factor and Critical Crack Size

By using the assumptions for the correction factors F_s , F_w , F_e and F_g the stress intensity factor of a crack can be estimated for any nominal stress and crack length.

For eyebar U 35 - U 36 the measured dead load stress was 127 MPa (18.4 ksi) and the maximum measured live load stress was less than 7 MPa (1.0 ksi). The maximum total nominal stress was therefore 134 MPa (19.4 ksi). Figure 33 shows a plot of the stress intensity factor versus the size of a through crack (upper bound) and a corner crack (lower bound) in eyebar U 35 - U 36 if such cracks ever occur.

The critical crack size that could cause sudden brittle failure of the eyebar is that when the stress intensity factor, K , is equal to the fracture toughness, K_{Ic} , of the eyebar material. The

results of fracture toughness tests to date are shown in Fig. 34. The K_{Ic} values from the slow-bend specimens are plotted against the test temperature. Specimens were cut from the two eyebars taken from the Liberty Bridge. The curve in the figure is arbitrarily drawn, based on comparison with fracture toughness data from the Carquinez West Bridge which also has AISI 1035 heat-treated eyebars²². At a temperature of -40° F. the average value for the fracture toughness of the Liberty Bridge eyebars is estimated to be $76 \text{ MPa } \sqrt{\text{m}}$ ($69 \text{ ksi } \sqrt{\text{in.}}$ from Fig. 34. The corresponding critical crack size for failure is calculated to be 7.9 mm (0.31 in.) for the through crack. For the lower bound case of a corner crack, no brittle fracture would be expected before the crack grew to 47.6 mm (1.875 in.) and through the thickness of the eyebar.

4.2 Fatigue Strength

The brittle fracture critical crack size in eyebar heads could be arrived at through fatigue crack growth, stress corrosion or corrosion fatigue¹⁶. While work is in progress to study the sensitivity of the eyebar material to stress corrosion and corrosion fatigue, preliminary evaluations based on results from related studies²³ indicated that these would not be the governing factors. The behavior of fatigue crack growth in eyebar heads when subjected to traffic loading is therefore of primary concern.

The fracture mechanics approach to fatigue crack growth relates the crack growth rate, da/dN , to the stress intensity factor²⁴. The governing equation is of the form:

$$\frac{da}{dN} = C (\Delta K)^n \quad (4.5)$$

where C and n are empirical constants for a given material and ΔK is the range of stress intensity factor. This model has been shown to describe fatigue crack growth in structural members^{25,26,27,28} in the range of $10^{-7} < da/dN < 10^{-3}$ mm/cycle. In practical applications, Eq. 4.5 is rearranged to give the number of cycles for an initial flaw of size a_i to reach a critical or final flaw size, a_f .

$$N = \frac{1}{C} \int_{a_i}^{a_f} \frac{da}{(\Delta K)^n} \quad (4.6)$$

or for numerical integration^{14,21,29};

$$N = \frac{1}{C} \sum_{j=1}^m \frac{1}{(\Delta K)^n} \Delta a_j \quad (4.7)$$

The range of the stress intensity factor, ΔK , is given by:

$$\Delta K = F_s \times F_w \times F_e \times F_g \times S_r \times \sqrt{\pi a} \quad (4.8)$$

where F_s , F_w , F_e and F_g are the individual correction factors as described before, S_r is the nominal stress range corresponding to the

live load stress variation, and a is the crack length. The constants C and n can be taken as $C = 2.0 \times 10^{-10}$ and $n = 3$ with da/dN in inches per cycle²⁵.

Equations 4.6, 4.7 and 4.8 apply only to constant amplitude cyclic loads in the range of crack growth rates of 10^{-7} to 10^{-3} mm/cycle (4×10^{-9} to 4×10^{-5} in/cycle). In the range of very low crack growth rates, it is generally recognized that there exists a threshold stress intensity factor below which cracks would not grow. The threshold value for ferrite-pearlite structural steels may be taken as $3.3 \text{ MPa } \sqrt{m}$ ($3.0 \text{ ksi } \sqrt{\text{in.}}$)^{15,18}.

For the eyebars on the Liberty Bridge the highest live load stress is below 10 MPa (1.5 ksi) which was measured at the most highly stressed eyebars, U 46 - U 47, under a very high live load of 552 kN (124 kips). With an assumed flaw size of 1.14 mm (0.045 in.) and a 10 MPa (1.5 ksi) stress range, the computed stress intensity factor range is $2.47 \text{ MPa } \sqrt{m}$ ($2.25 \text{ ksi } \sqrt{\text{in.}}$). This is below the threshold value, therefore, no crack growth would be anticipated.

If a flaw size of 3.18 mm (0.125 in.) is developed by corrosion, the corresponding ΔK would be at the threshold of fatigue crack growth for a live load stress range of 10 MPa (1.5 ksi). By assuming that this hypothetical condition would cause the crack to grow, the application of Eq. 4.8 resulted in a fatigue life of approximately ten million cycles for a through crack to reach the critical crack size for failure. Of course, this value was computed on the assumption of a very large initial flaw size ((3.18 mm (0.125 in.))

for a through crack and is therefore considered a very conservative estimate.

More realistically, because the most conservatively estimated stress intensity factor range is below the fatigue crack growth threshold value, no cracks would be anticipated to grow in the eyebar heads.

5. DISCUSSION

5.1 Stress Evaluation

In order to evaluate the fracture resistance and fatigue strength of the bridge, dead load and live load stresses in the most critical members must be accurately calculated. Accuracy is, however, difficult to achieve because of the necessary approximations in the stress analysis. The assumption of point loads (dead load and live load), frictionless joints, and planar trusses all contribute to the uncertainty. Furthermore, the computation of local stresses from nominal member forces relies on the adequacy of proper modelling.

While the local stress concentrations in eyebar heads were correlated for computed and measured values, the forces in the eyebars due to live load and dead load have not yet been computed very satisfactorily. It appears that the consideration of the continuous deck and the lateral bracing system in a three dimensional structural analysis is necessary.

During the removal of eyebars U 35 - U 36A and D, strain measurements were taken at the adjacent floor beams and stringers. Results showed little stress transfer between eyebars, deck and stringers, but the floor beam was subjected to lateral bending. Although this condition does not exist when the bridge is under vehicular load, an analysis of the load transfer in eyebar removal

would provide some information for an overall stress analysis of the bridge.

5.2 Bonded Eyebars Heads

During the removal of eyebars U 35 - U 36A and D it was found that forces in eyebar heads on lapping eyebars were bonded together because of corrosion. Indication of this bonding condition include the appearance of the contacting surfaces, the relatively loud noise when the lapping heads separate under load, the difficulties in separating some of the heads, and the measured stress distribution pattern in the heads.

The bonding of eyebar head faces rendered the adjoining eyebars, such as U 34 - U 35 and U 35 - U 36, continuous members similar to lap joints. The tension force in one eyebar could be transferred through shear to the other. The result was a decrease in stress concentration at the pin hole. The stress magnitudes in the eyebar heads were about the same as in the eyebar shanks. This condition was observed in all the eyebar heads where strains were measured.

Reduction of the stress concentration in eyebar head pin holes due to bond decreased the maximum stress at the pin hole edge. The corresponding stress intensity factor range, ΔK , was found to be below the threshold value of $3.3 \text{ MPa } \sqrt{\text{m}}$ ($3.0 \text{ ksi } \sqrt{\text{in.}}$). This would be so even for the upper bound case of through cracks. Through the thickness flaws 3.18 mm (0.125 in.) in size, if developed, would not

be expected to propagate at all. With an estimated critical flaw size much larger than the possible size of non-propagating initial flaws, it is not likely that any danger of brittle fracture will result.

5.3 Anticipated Conditions

With the assumption that the dead weight of the deck system will not be increased, the members of the existing trusses will have sufficient capacity to carry the intended loads according to results of this analysis. The live load stresses were lower than computed values and are expected to remain so, since no change in traffic pattern is anticipated after rehabilitation of the bridge. Based on these loads, and the results of the fracture resistance, it can be stated that fracture will not occur.

Since all members which are made up of eyebars have four or more bars, there is no non-redundant eyebars. Adding to this condition that there are no fracture critical eyebar heads, the fracture resistance and fatigue strength of the bridge are considered adequate for the projected life of the rehabilitated structure.

6. CONCLUSIONS AND RECOMMENDATIONS

Based on the results of eyebars head stress distribution analysis, by the finite element method, the following conclusions can be drawn:

1. Within the limits of design specifications (AISC, AASHTO, AREA) eyebars with moderate transition from the head to shank have the highest stress at the pin hole edge on a transverse diameter at the pin hole.
2. The computed stresses in the head of a test eybar correlated very well with measured values, confirming the accuracy of the analysis (Fig. 25).
3. The dominate factor governing the stress concentration at the pin hole is the ratio of a/b , a being the width of the head and b the width of the eybar shank. (Figs. 28 and 29). Other factors such as the ratio of pin hole diameter to eybar width (d/b) and the ratio of width to thickness (b/t), only affect the stress concentration factor slightly.
4. Within the specified width ratios $a/b = 0.665$ to 0.75 , the highest stress concentration factor is about 3.5, calculated against the nominal stress in the shank and from a fine mesh finite element analysis. This value could be used as a nominal value of SCF for the design of eyebars against fatigue and fracture.

From the field studies on the Liberty Bridge, the following can be summarized:

5. The eyebar head pin holes appeared to be in good condition. No cracks or severe notches were found in the eyebar heads which were inspected. However, there were some corroded spots in the pins between eyebar heads.

6. Live load stresses were very low in all eyebars on which strain gages were mounted. The highest magnitude under a live load of 552 kN (124 kips) was less than 10 MPa (1.5 ksi), Table 1.

7. The live load strain rate for the eyebars was in the order of 5 to 10 seconds, from zero to maximum strain, Fig. 6, corresponding to a static condition.

8. Live load stress distributions within eyebar groups were not exactly uniform among the bars, Fig. 7.

9. Stress distribution in eyebar heads agreed with the computed pattern in one case, Fig. 25. In all other cases the actual stress concentration was much lower than predicted, Figs. 12 through 15.

10. Eyebars head faces were found to adhere to each other due to corrosion. This condition made the removal of eyebars difficult. It also permitted transfer of forces directly from one eyebar to the adjacent eyebar in the manner of a lap-joint. The consequence was the reduced stress concentration at pin holes.

From the fracture resistance and fatigue strength evaluation a few conclusions are made:

11. A through-the-thickness crack at the pin hole is more serious than a corner crack at the edge of the pin hole, Fig. 31. Due to the corrosion effect, flaws would more likely develop at the corners first.

12. The average fracture toughness, K_{Ic} , of the eyebars (AISI 1035 heat-treated steel) is $76 \text{ MPa } \sqrt{\text{m}}$ ($69 \text{ ksi } \sqrt{\text{in.}}$) at -40° C. (-40° F.) obtained from slow bend test results. More tests are planned to be conducted.

13. Based on this fracture toughness value, the critical through-crack which would cause brittle fracture of the eyebars at -40° C. (-40° F.) was found to be 7.9 mm (0.31 in.). The corner crack would not cause failure until it grew through the thickness 47.6 mm (1.875 in.).

14. The stress intensity factor ranges are below the threshold value for assumed initial flaw sizes and anticipated live load stress range. For a 1.14 mm (0.045 in.) initial through-the-thickness flaw no crack growth would occur. For a 3.18 mm (0.125 in.) flaw of the same shape, it is estimated that approximately ten million cycles are required for the crack to reach the critical size.

While analysis and evaluation are still in progress, it can be concluded, based on results to date, that the Liberty Bridge should be able to carry the anticipated loads. Rehabilitation of the bridge, as planned, is recommended.

NOMENCLATURE

a	distance from pin hole to outside edge of eyebar head
a	crack length
a_i	initial flaw size
a_f	final flaw size
b	width of eyebar shank
d	pin diameter
n	constant in crack growth equation
r_i	inside radius of eyebar head
r_o	outside radius of eyebar head
r_t	radius of transition from eyebar head to shank
A	bearing area of pin on pinhole
C	material constant in crack growth equation
E	modulus of elasticity
F_s	front free surface correction factor
F_w	finite width correction factor
F_e	crack shape correction factor
F_g	stress gradient correction factor
K	stress intensity factor
K_r	radial stiffness of boundary elements
K_t	tangential stiffness of boundary elements

NOMENCLATURE (continued)

K_{tj}	average stress concentration over the increment of fatigue crack growth
K_{Ic}	static fracture toughness
N	number of cycles for a flaw to grow from an initial size to a final size
S_r	nominal stress range in the eyebar shank
SCF	stress concentration factor
W	width of the detail
da/dN	rate of fatigue crack growth
Δa_j	incremental crack size for fatigue crack growth
ΔK	stress intensity factor range
σ	nominal stress in eyebar
σ_{ys}	yield stress

TABLE 1

MAXIMUM MEASURED STRESS RANGE IN EYEBAR SHANKS

Gage	Location	Maximum Live Load Stress	
		(ksi)	(MPa)
35	U 34 - 35A, Top	1.05	7.24
36	U 34 - 35A, Bottom	0.66	4.55
39	U 34 - 35B, Top	0.94	6.48
40	U 34 - 35B, Bottom	0.64	4.41
43	U 34 - 35C, Top	1.07	7.38
44	U 34 - 35C, Bottom	0.08	4.69
23	U 35 - 36A, Top	0.74	5.10
25	U 35 - 36B, Top	0.81	5.58
27	U 35 - 36C, Top	0.79	5.45
29	U 35 - 36D, Top	0.70	4.83
1	U 46 - 47A, Top	1.20	8.27
2	U 46 - 47A, Bottom	1.05	7.24
3	U 46 - 47B, Top	1.45	10.00
4	U 46 - 47B, Bottom	1.18	8.14
5	U 46 - 47C, Top	1.22	8.41
6	U 46 - 47C, Bottom	1.16	8.00
23	U 47 - 48A, Top	1.07	7.38
24	U 47 - 48A, Bottom	0.57	3.93
25	U 47 - 48B, Top	0.92	6.34
26	U 47 - 48B, Bottom	0.58	4.00
29	U 47 - 48D, Top	0.95	6.55
30	U 47 - 48D, Bottom	0.59	4.07
7A	U 48 - 49A, Top	1.32	9.10
8A	U 48 - 49C, Top	1.09	7.52
22A	U 48 - 49C, Top	1.42	9.79

TABLE 2

DESIGN CRITERIA FOR PROPORTIONING EYEBAR HEADS

	AISC	AASHTO	AREA
t	uniform ≥ 12.7 mm (0.5 in.)	uniform 12.7 to 50.8 mm (0.5 to 2.0 in.)	uniform
a	0.667b to 0.75b	≥ 0.675b	≥ 0.7b
b	≥ 8t	≥ 8t	
d _{pin}	≥ 0.875b	$\left[\frac{3}{4} + \frac{1}{4} \frac{\sigma_{ys}}{100,000} \right] b$	
d _{pin hole}	≥ 0.794 mm + d _{pin} (≥ 0.031 in. + d _{pin})		
r _t	≥ 2 r _o	≥ 2 r _o	

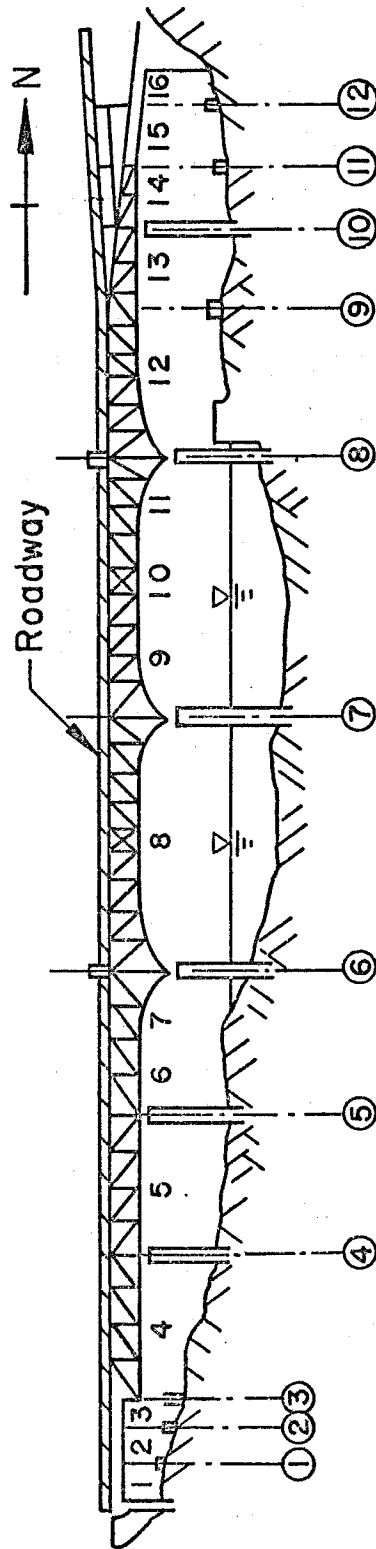


Fig. 1 Elevation of Liberty Bridge Looking West (Downstream)

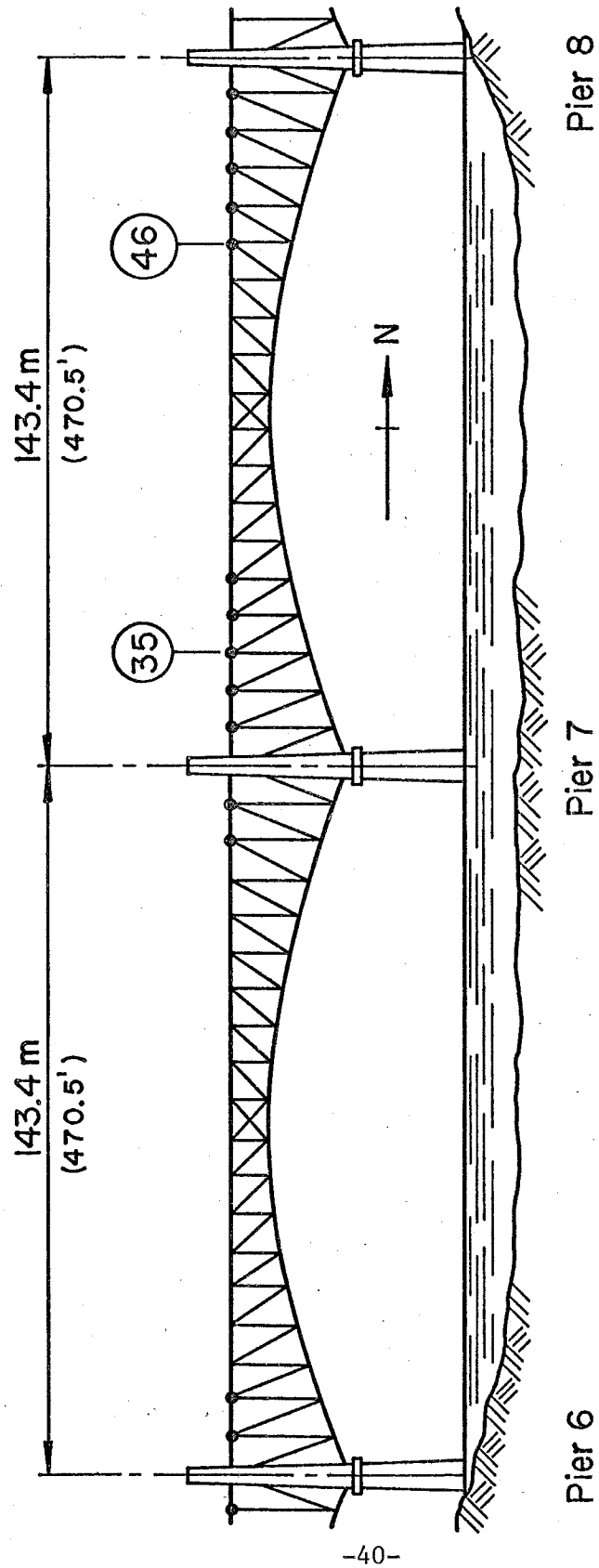


Fig. 2 Locations of Eyebars on the Main Spans Over the River

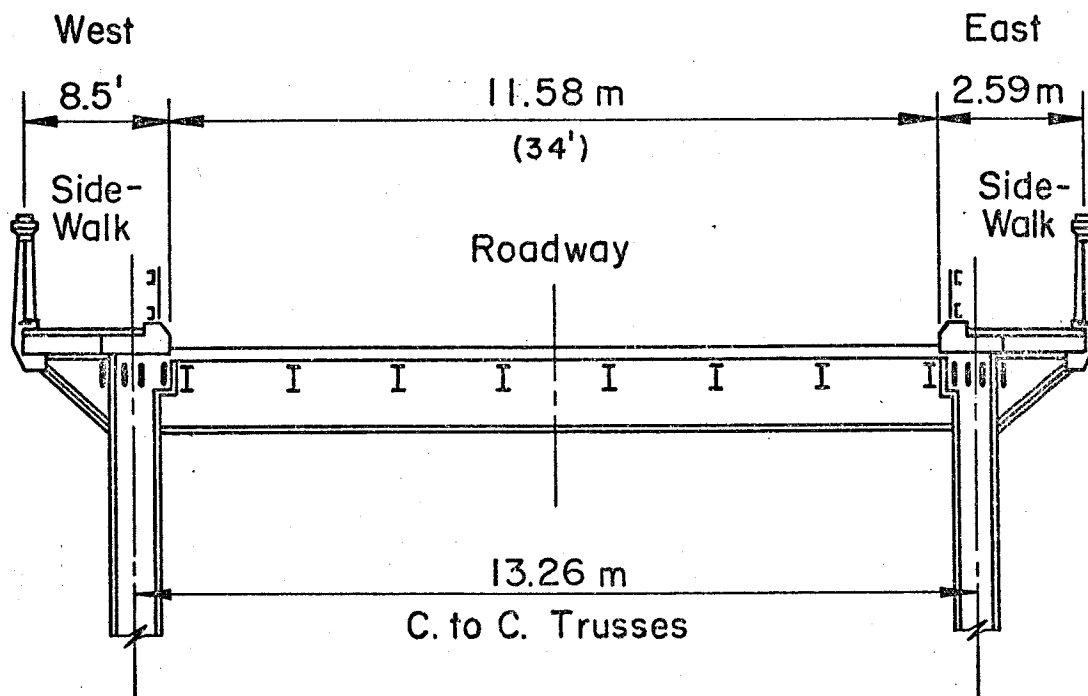


Fig. 3 Typical Cross Section of the Liberty
Bridge

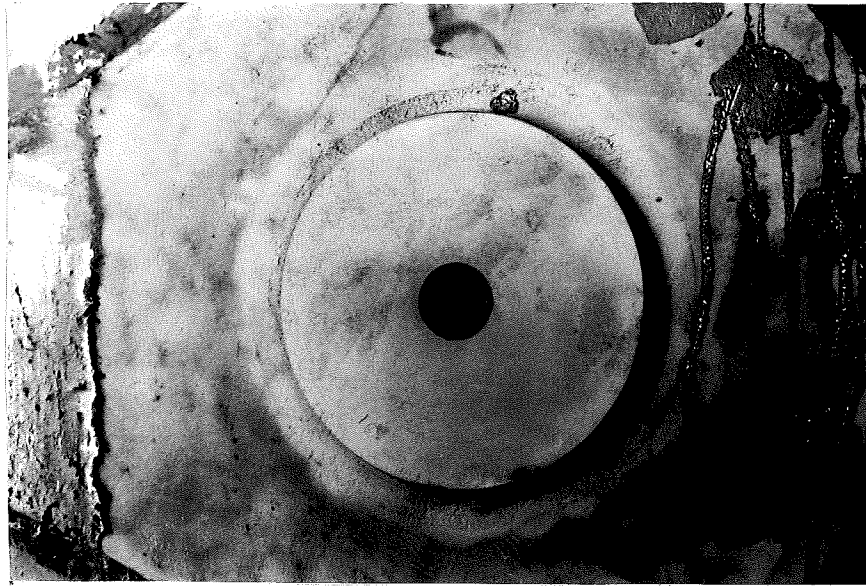


Fig. 4 Eyebar Head U 36A with Pin Cap Removed

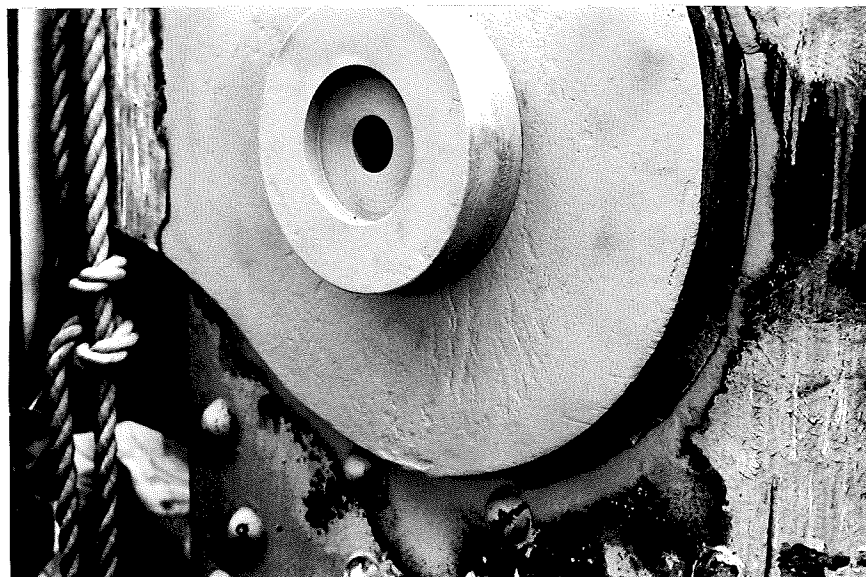


Fig. 5 Sandblasted Eyebar Head Showing Forging Marks

U34-35 (35)

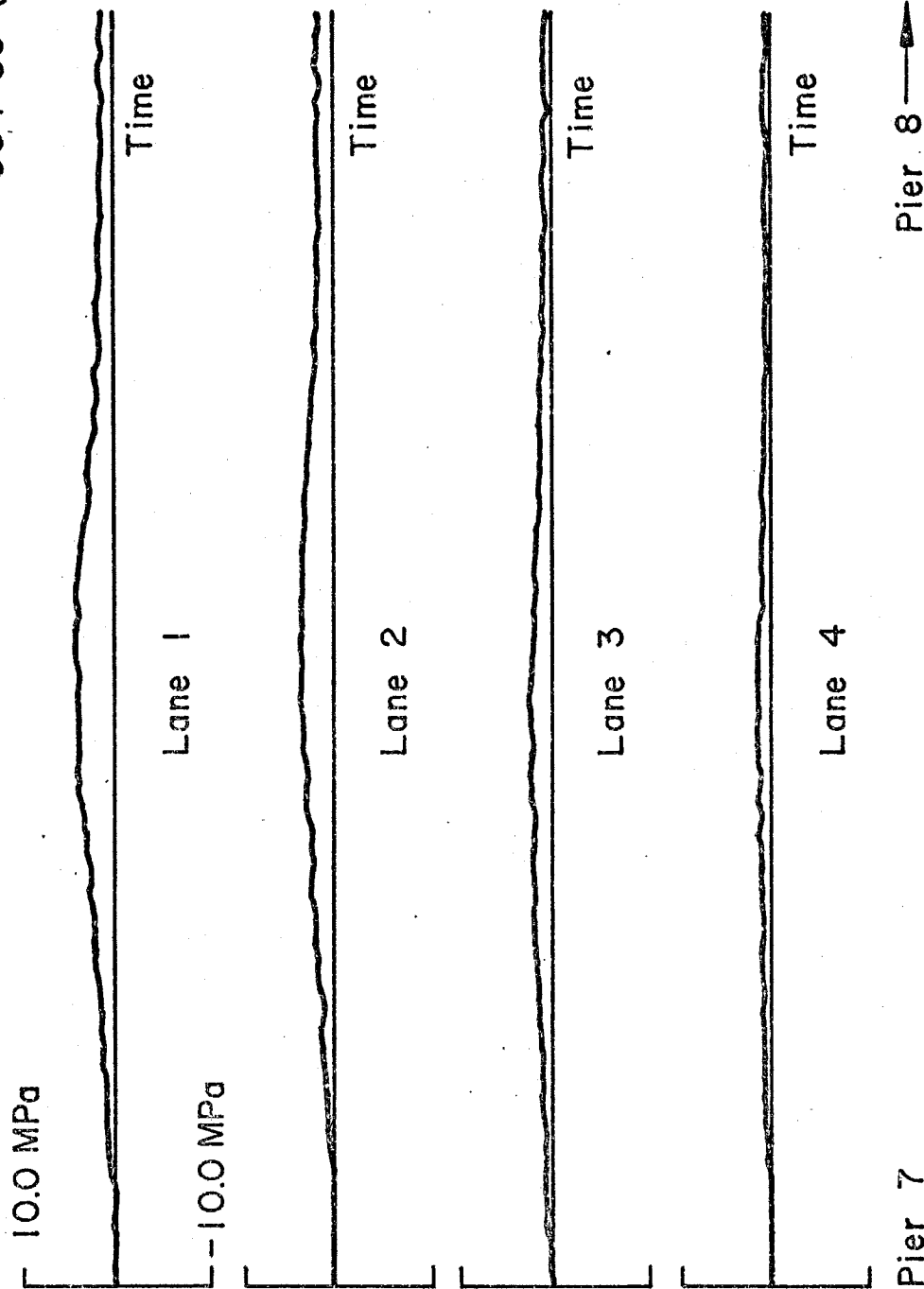
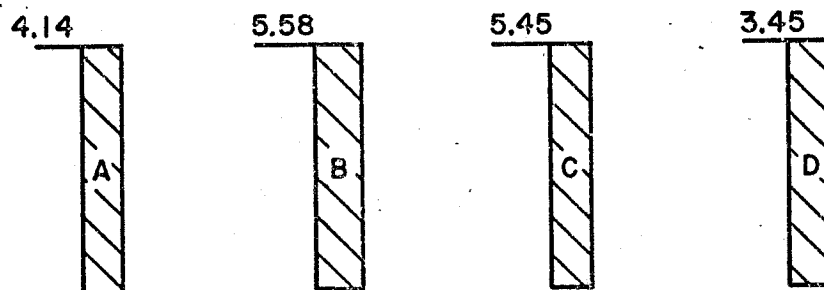
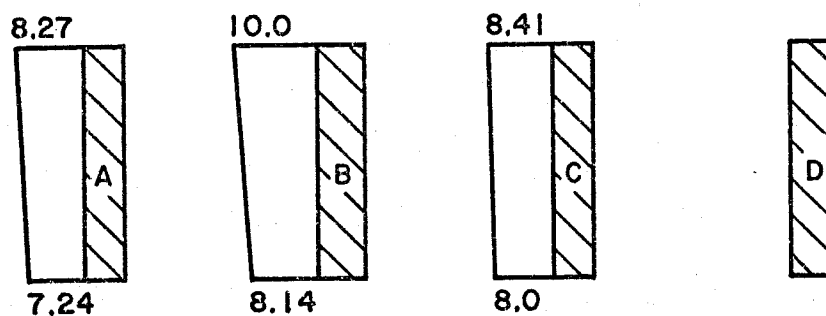


Fig. 6 Variation in Live Load Stress versus Time for Truck in Different Lanes



U 35-36



U 46-47

All Values In MPa

1 ksi = 6.895 MPa

Fig. 7 Measured Stress Ranges for Test Truck in Curb Lane,

Northbound

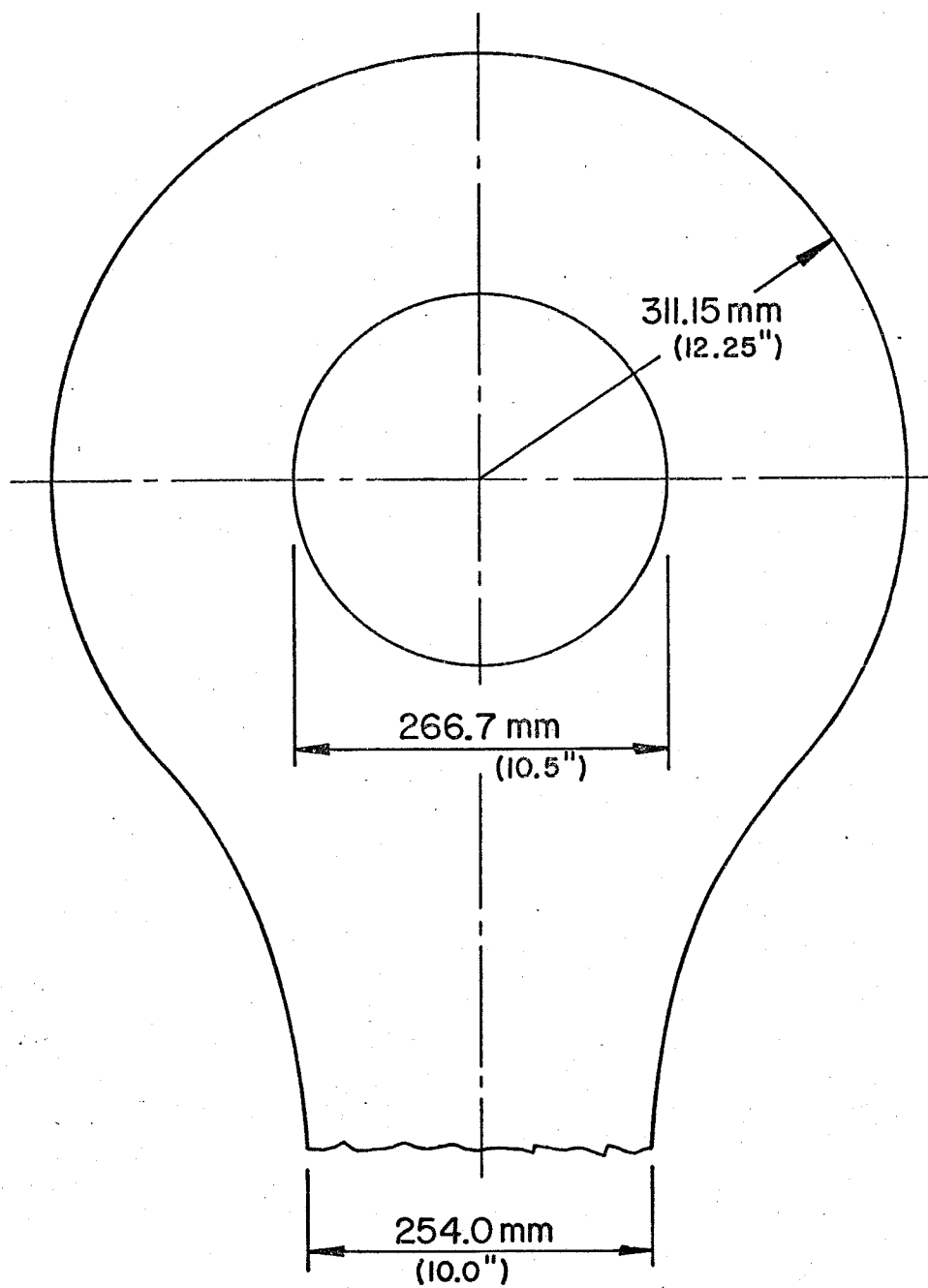


Fig. 8. Dimensions of Eyebars at U 35 - U 36

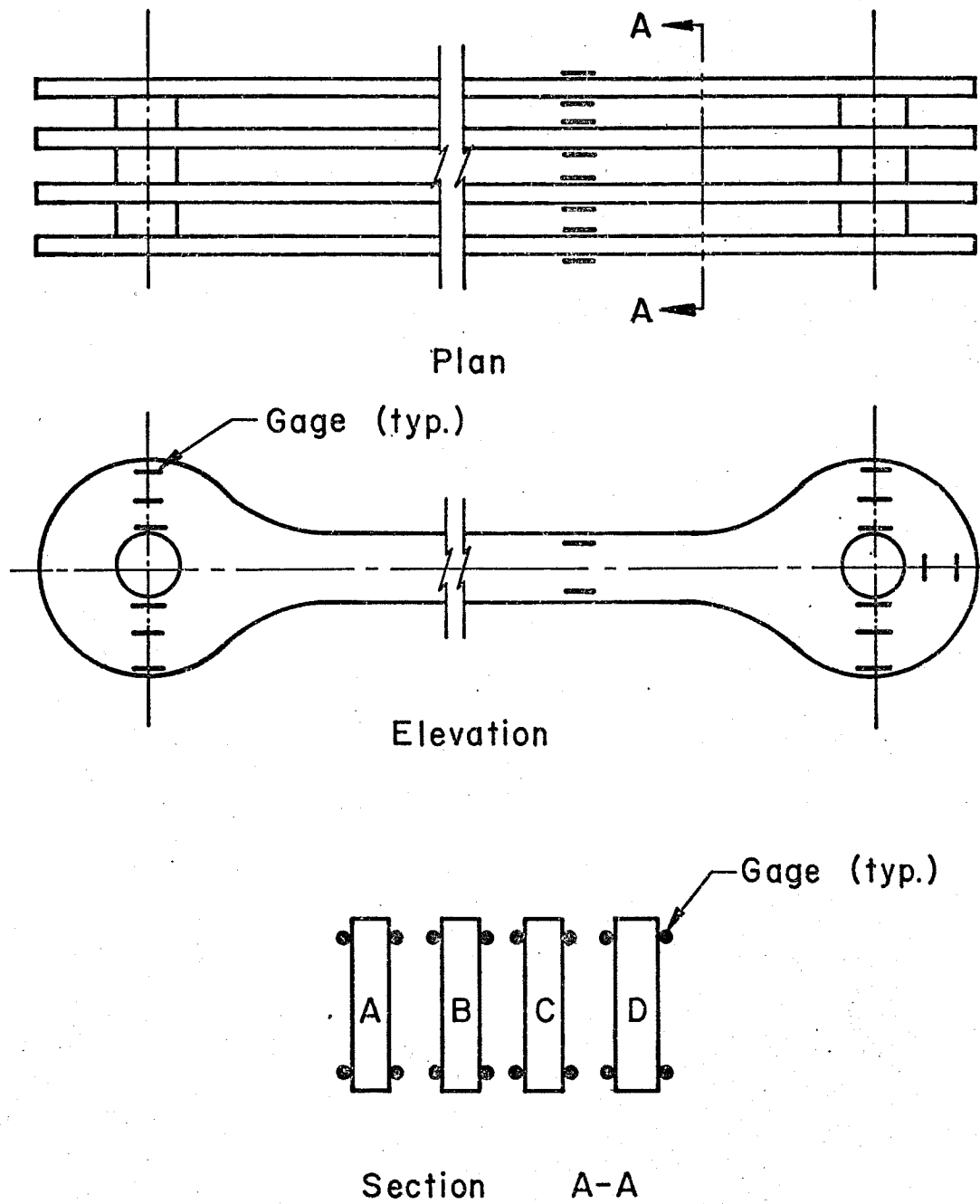


Fig. 9 Typical Arrangement of Strain Gages for Live
Load and Dead Load Study

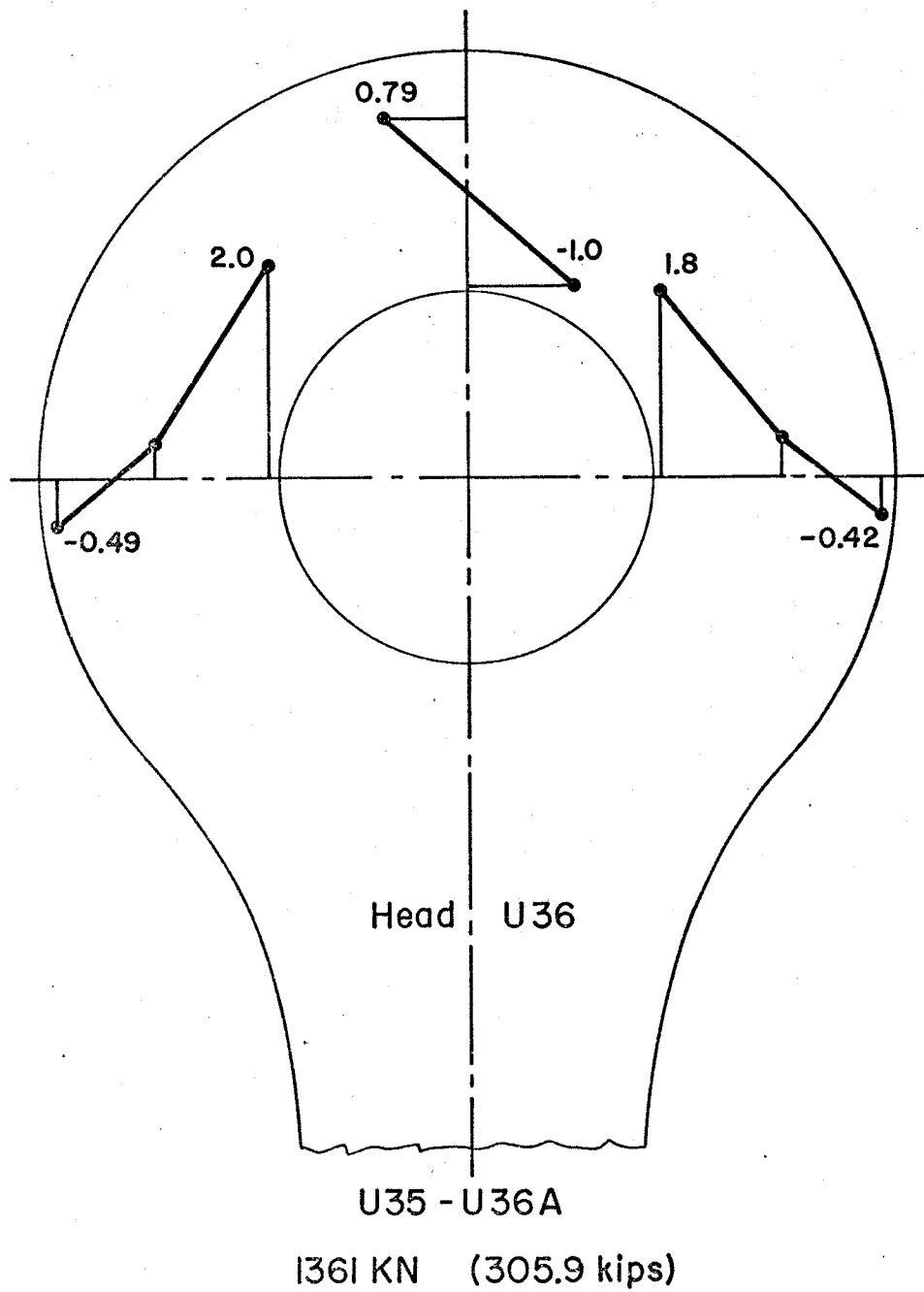


Fig. 10 Non-dimensionalized Measured Stress Distribution -

U 36A Dead Load

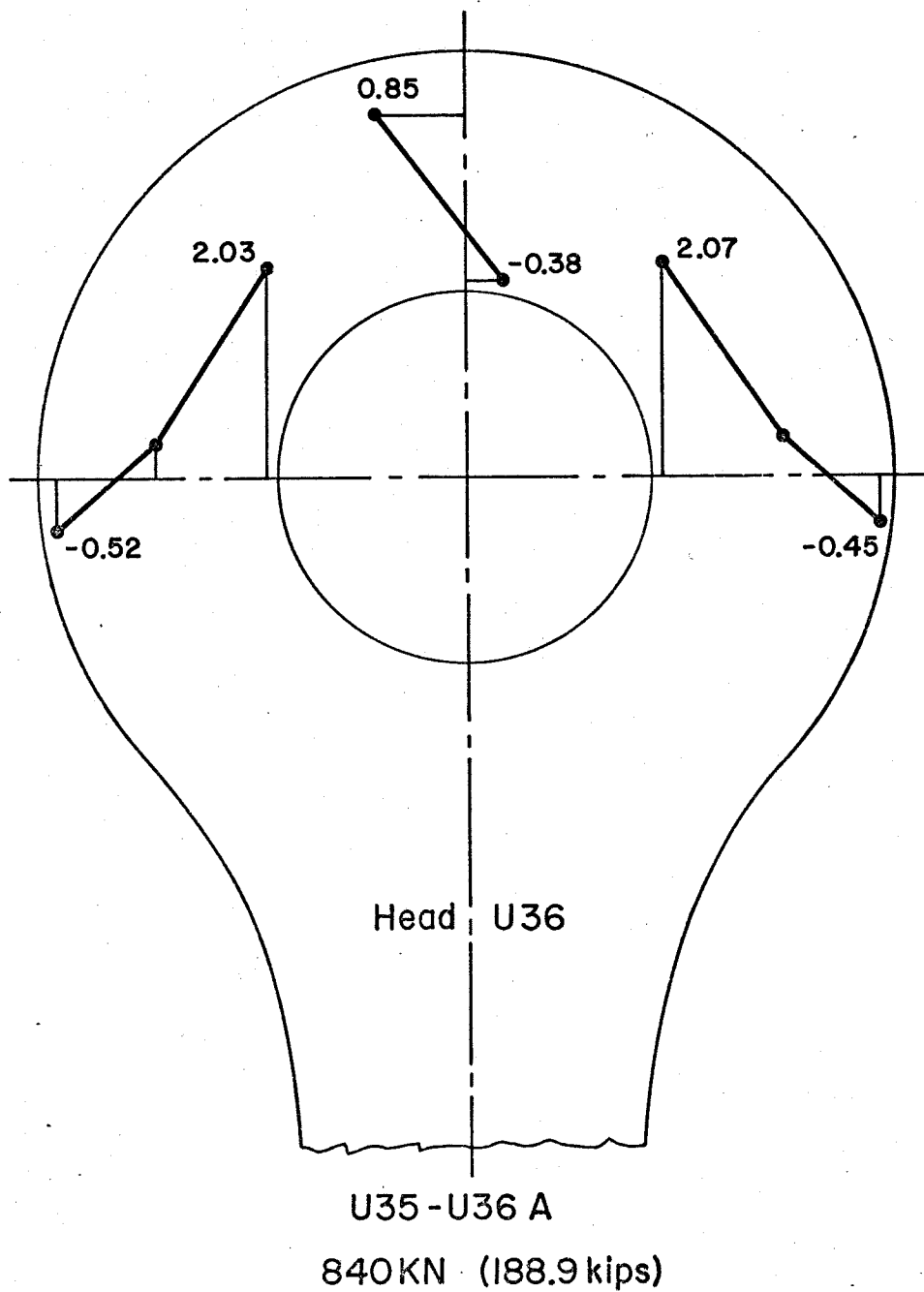
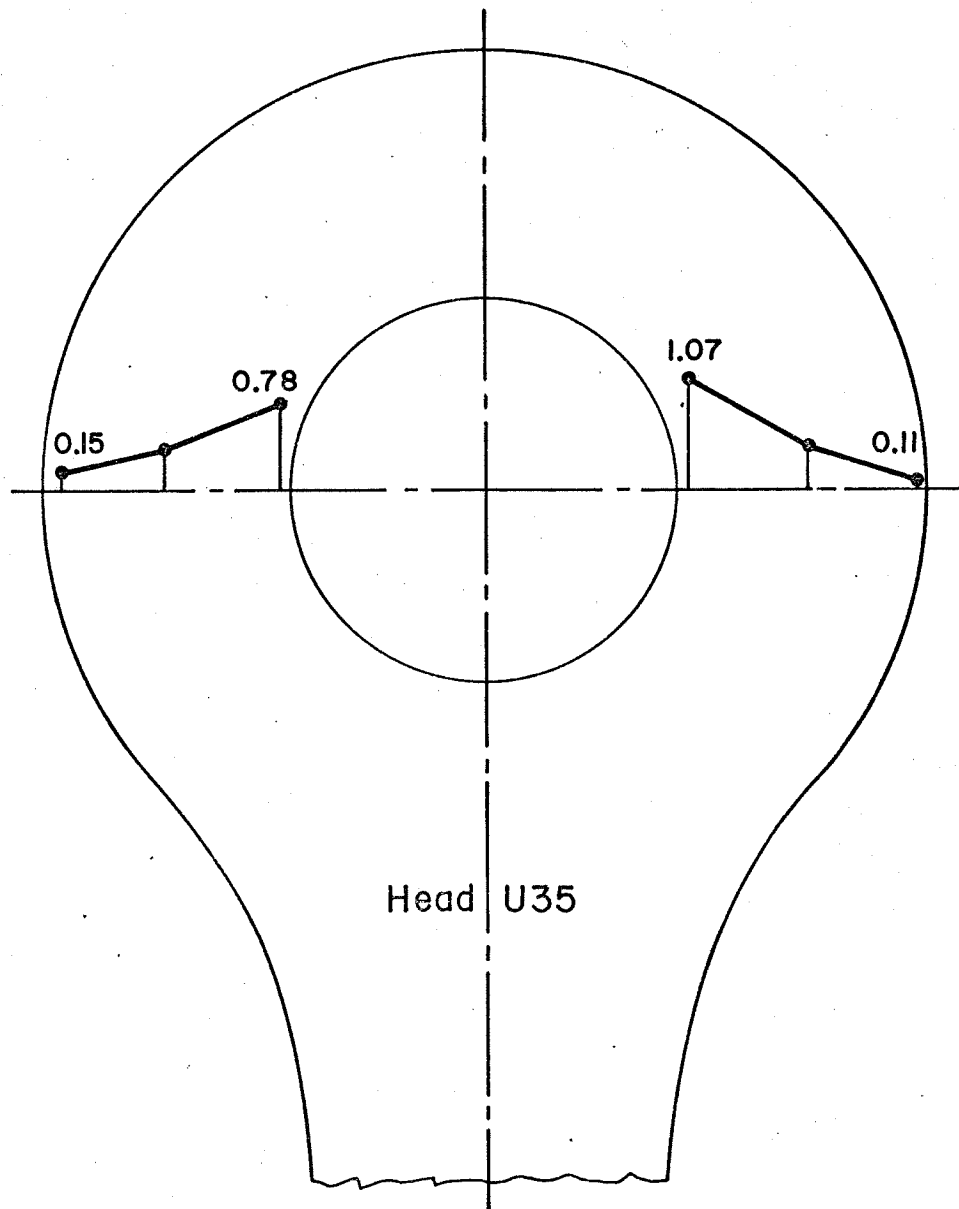


Fig. 11 Non-dimensionalized Measured Stress Distribution-

U 36A Partial Load



Head U35

U35 - U36A

1361 KN (305.9 kips)

Fig. 12 Non-dimensionalized Measured Stress Distribution -

U 35A Dead Load

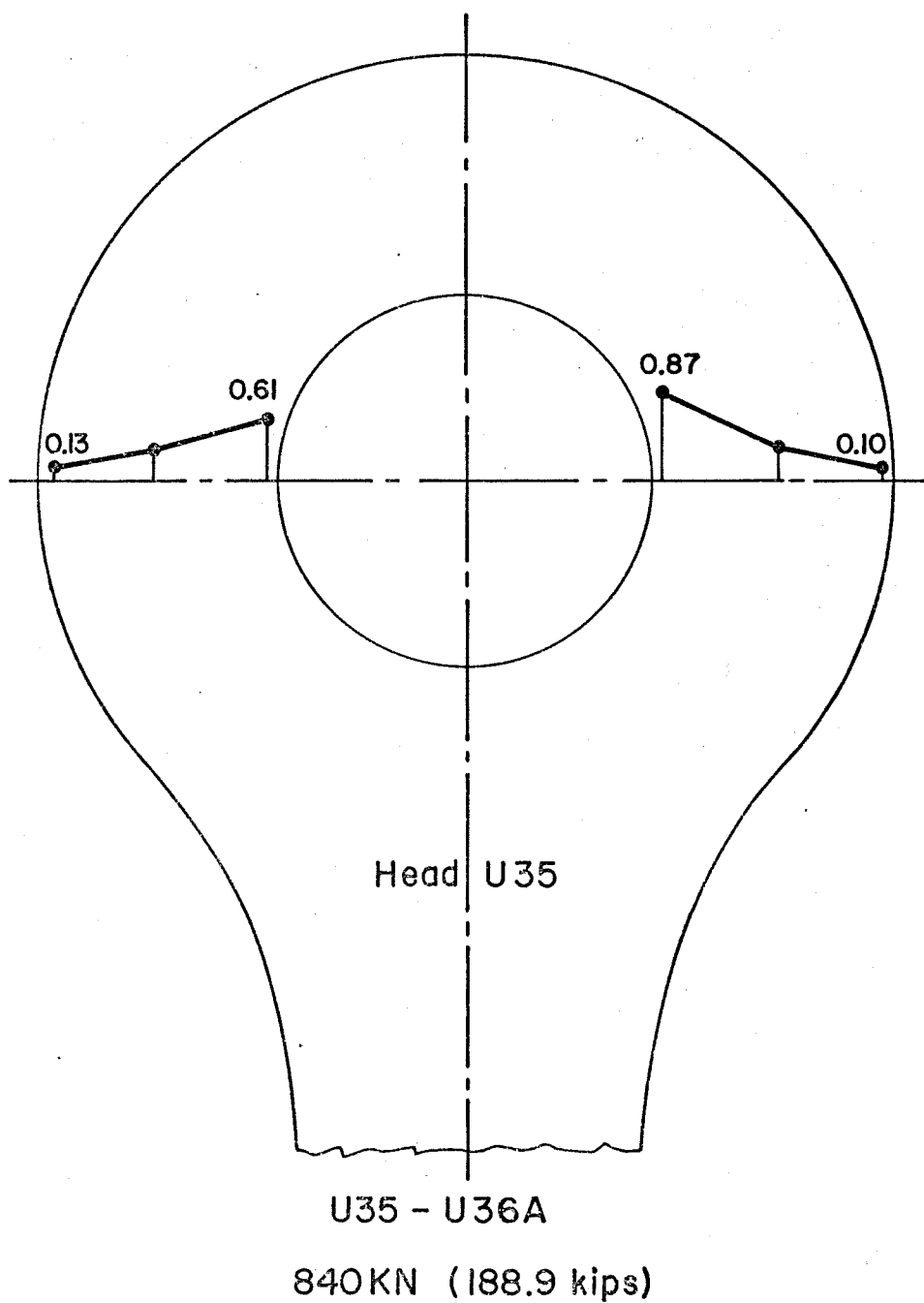


Fig. 13 Non-dimensionalized Measured Stress Distribution -

U 35A Partial Load

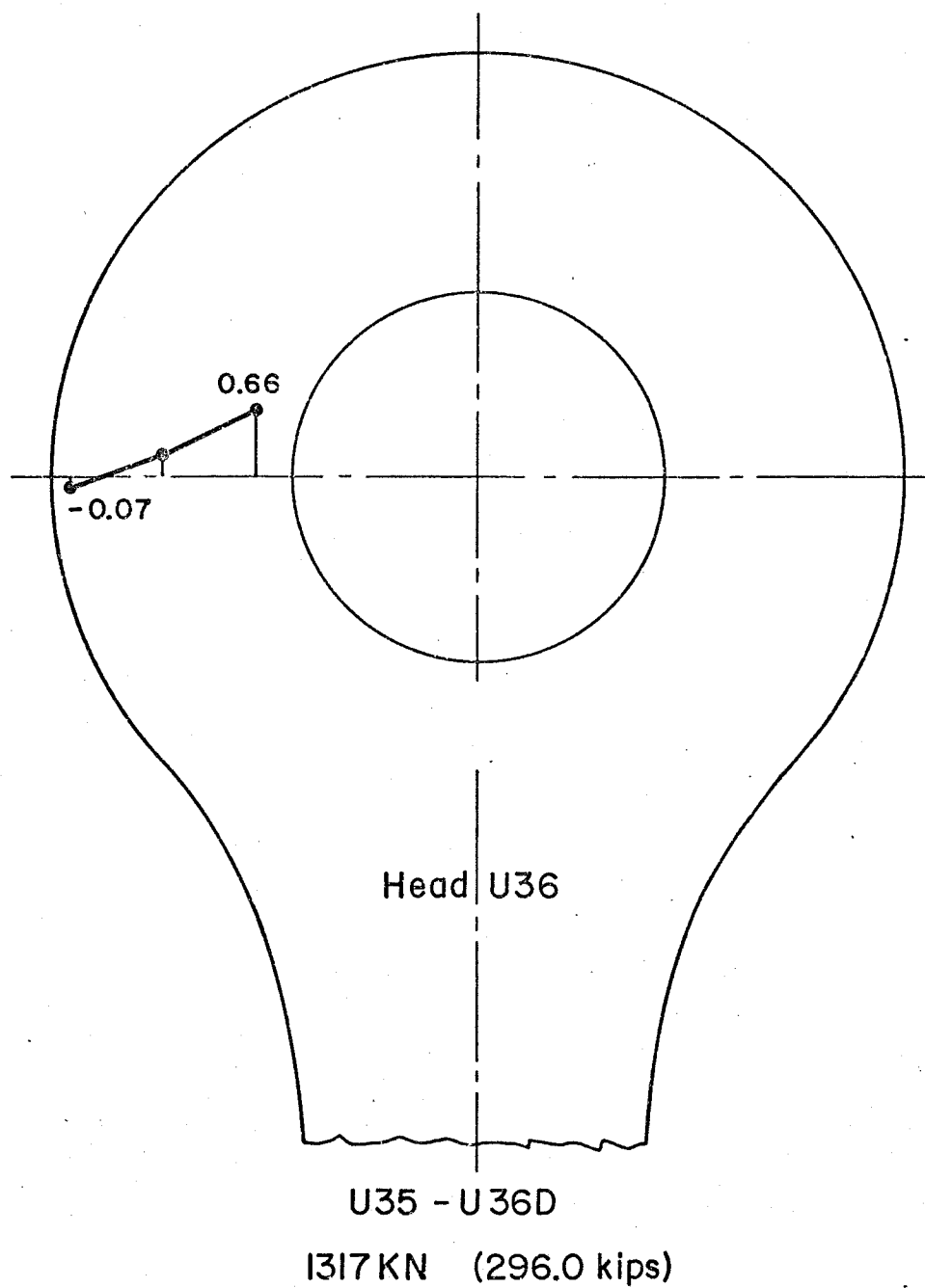


Fig. 14 Non-dimensionalized Measured Stress Distribution -

U 36D Dead Load

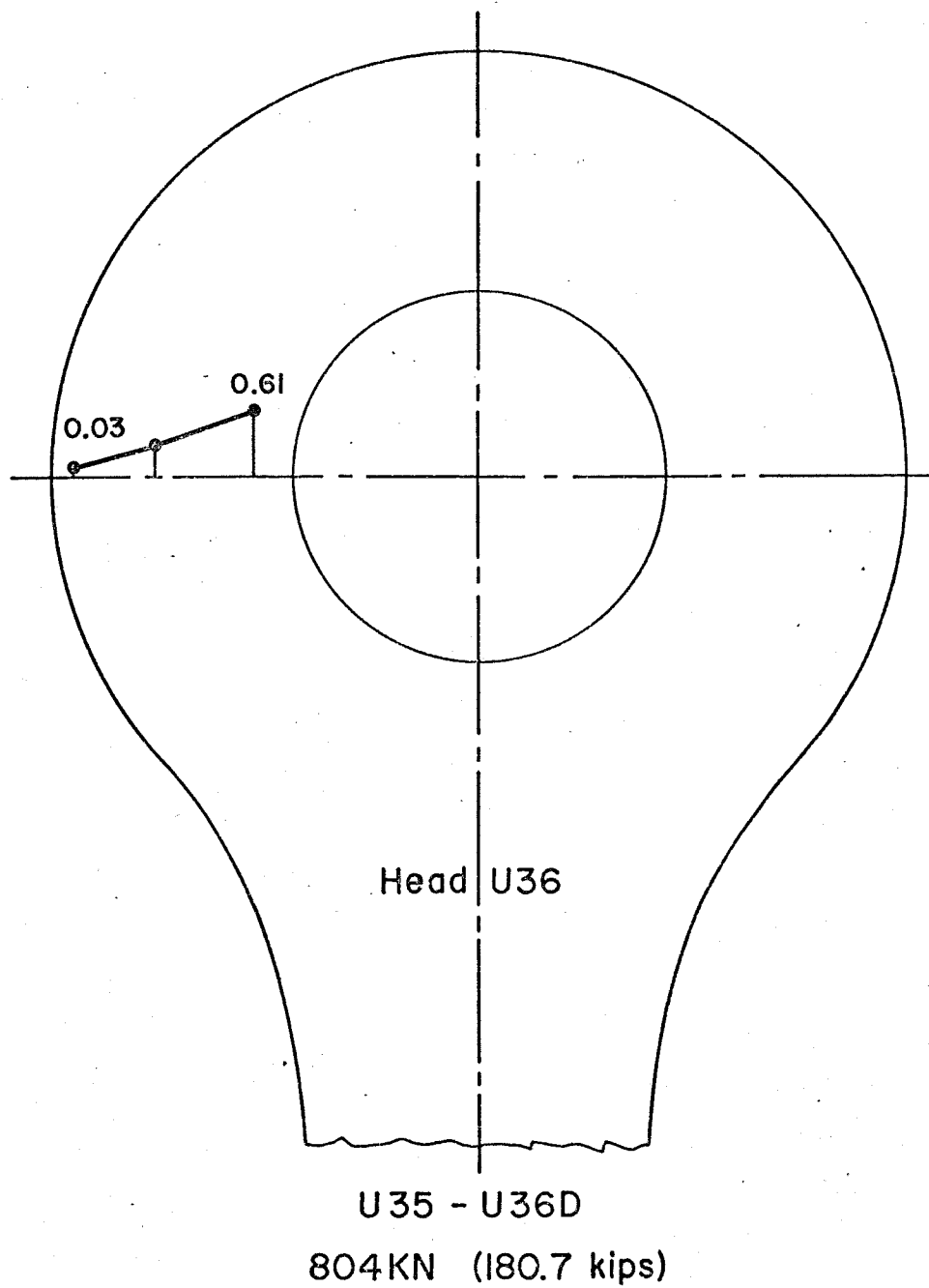
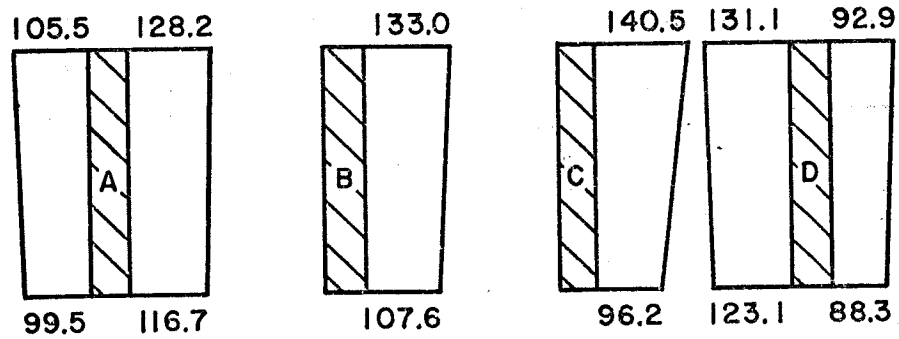
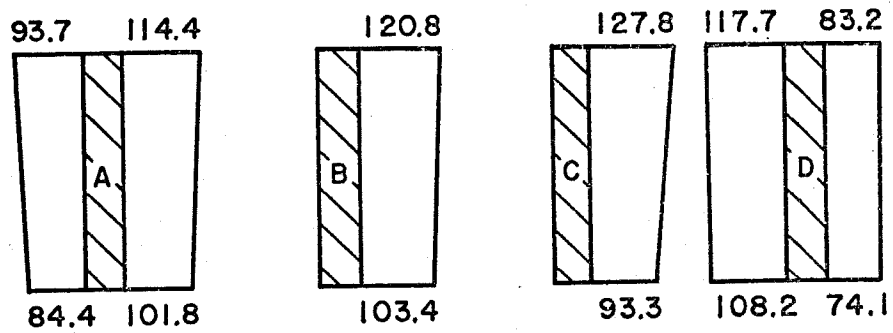


Fig. 15 Non-dimensionalized Measured Stress Distribution -

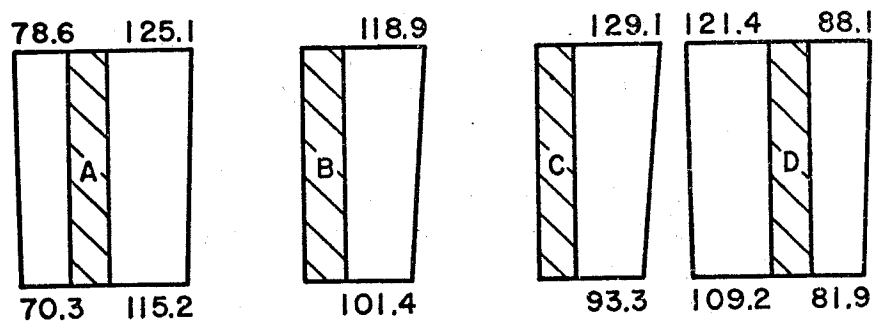
U 36D Partial Load



Unloading Eyebars



Loading Eyebars



Unloading Eyebars

All Values In MPa
1 ksi = 6.895 MPa

Fig. 16 Dead Load Stresses in Shanks of Eyebars

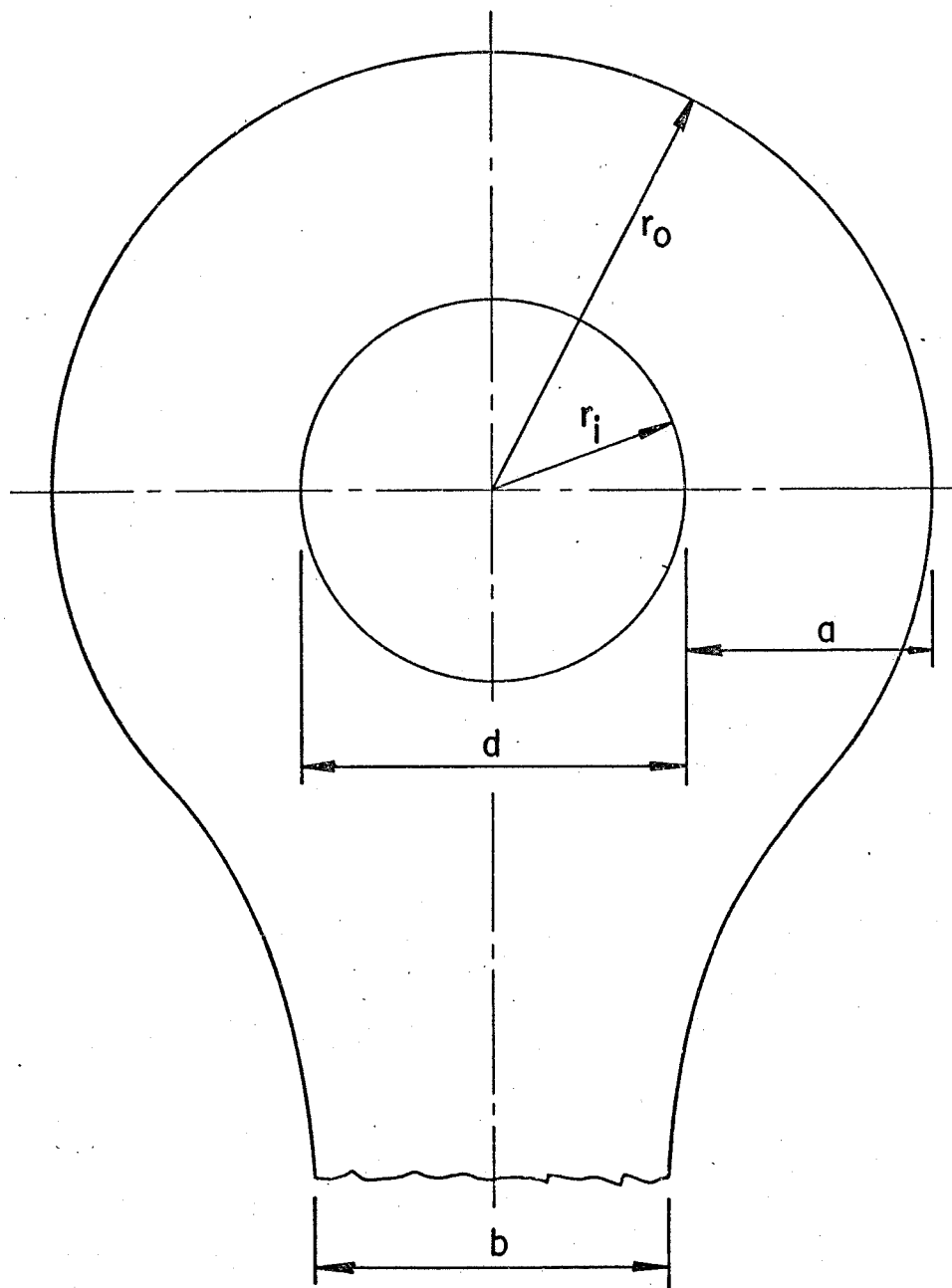


Fig. 17 Symbols Used to Describe Eyebar
Geometry

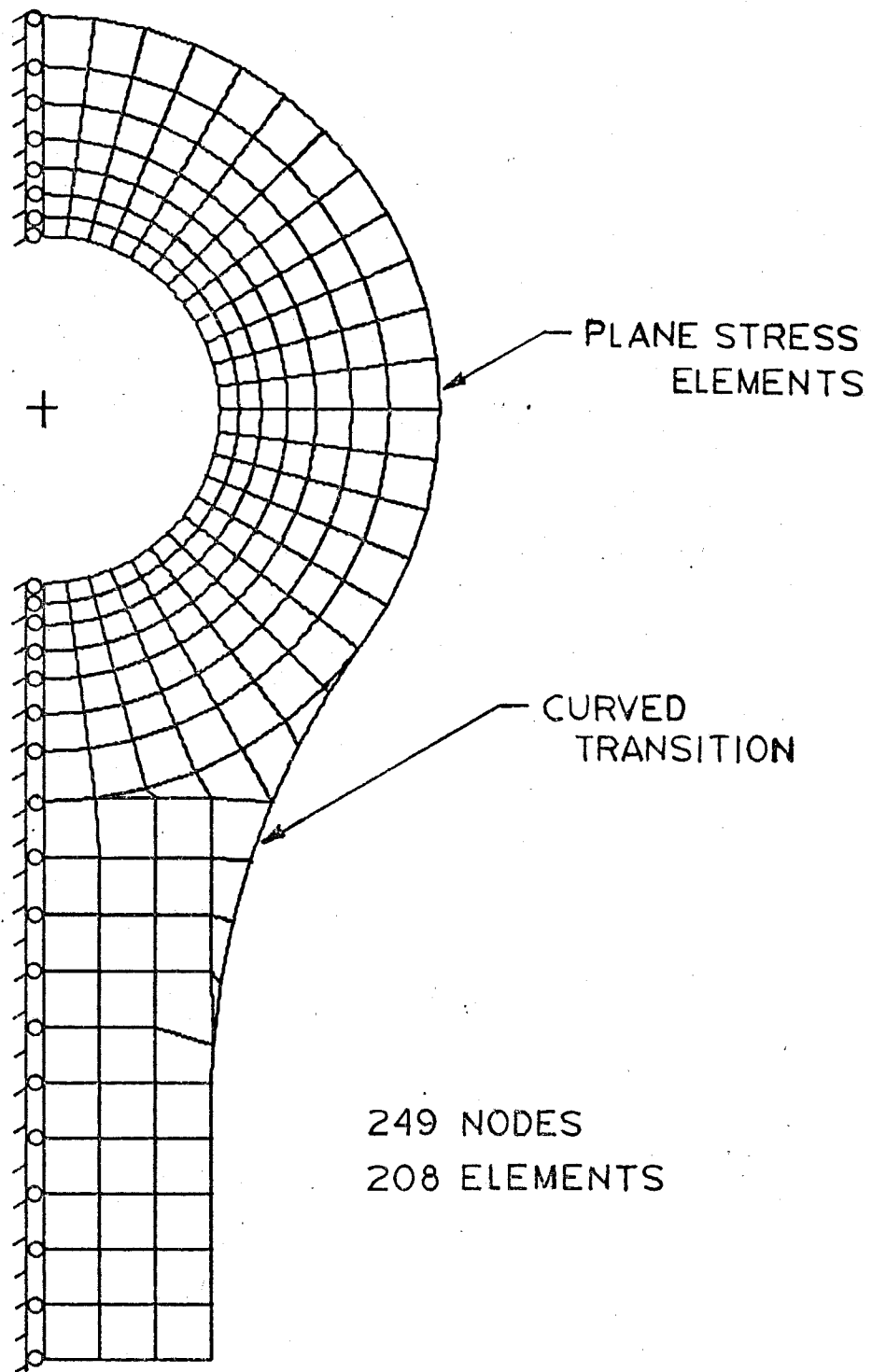


Fig. 18 Discretization of Eyebar Head With Curved Transition

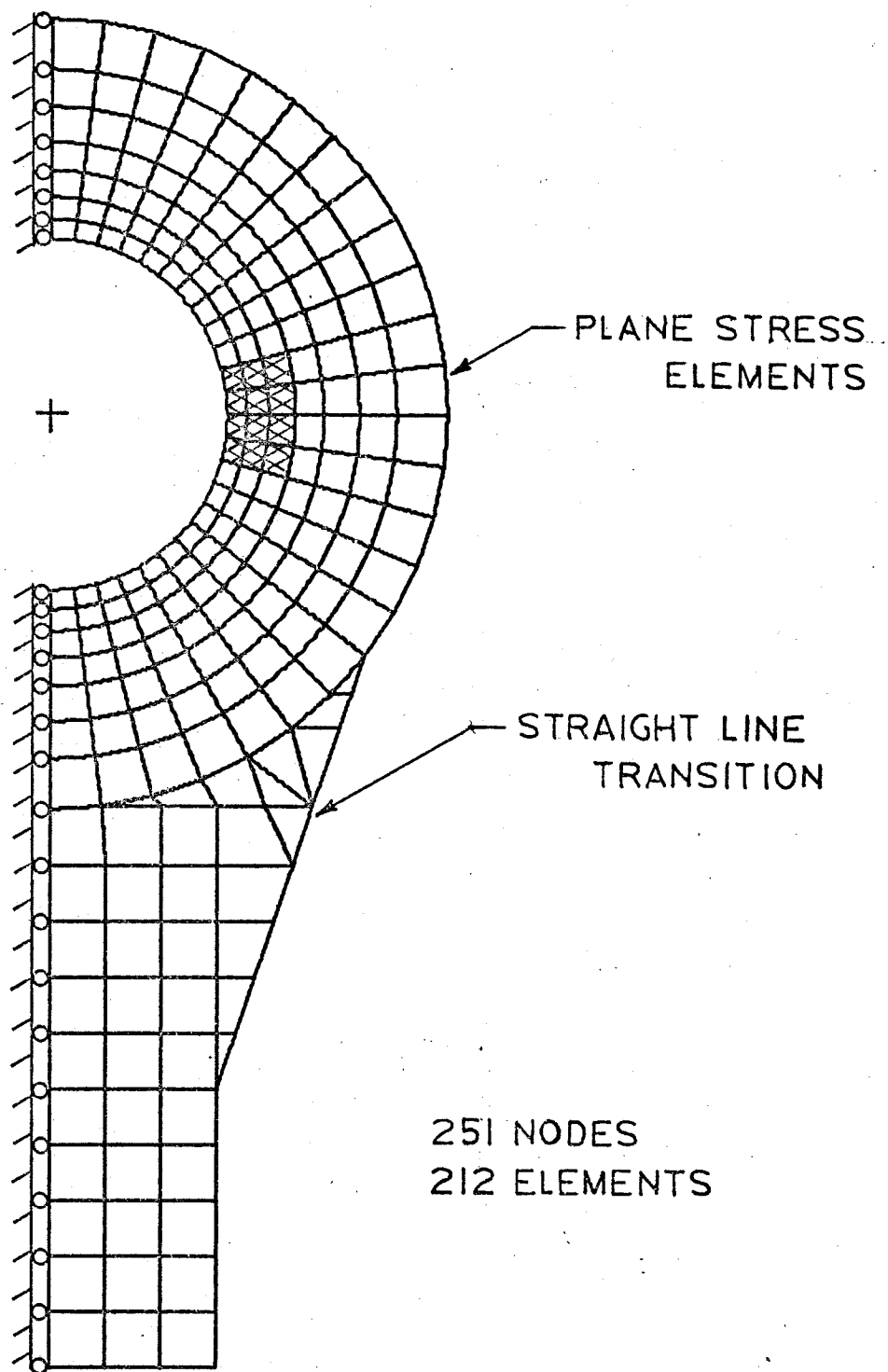


Fig. 19 Discretization of Eyebar Head with Straight

Line Approximation

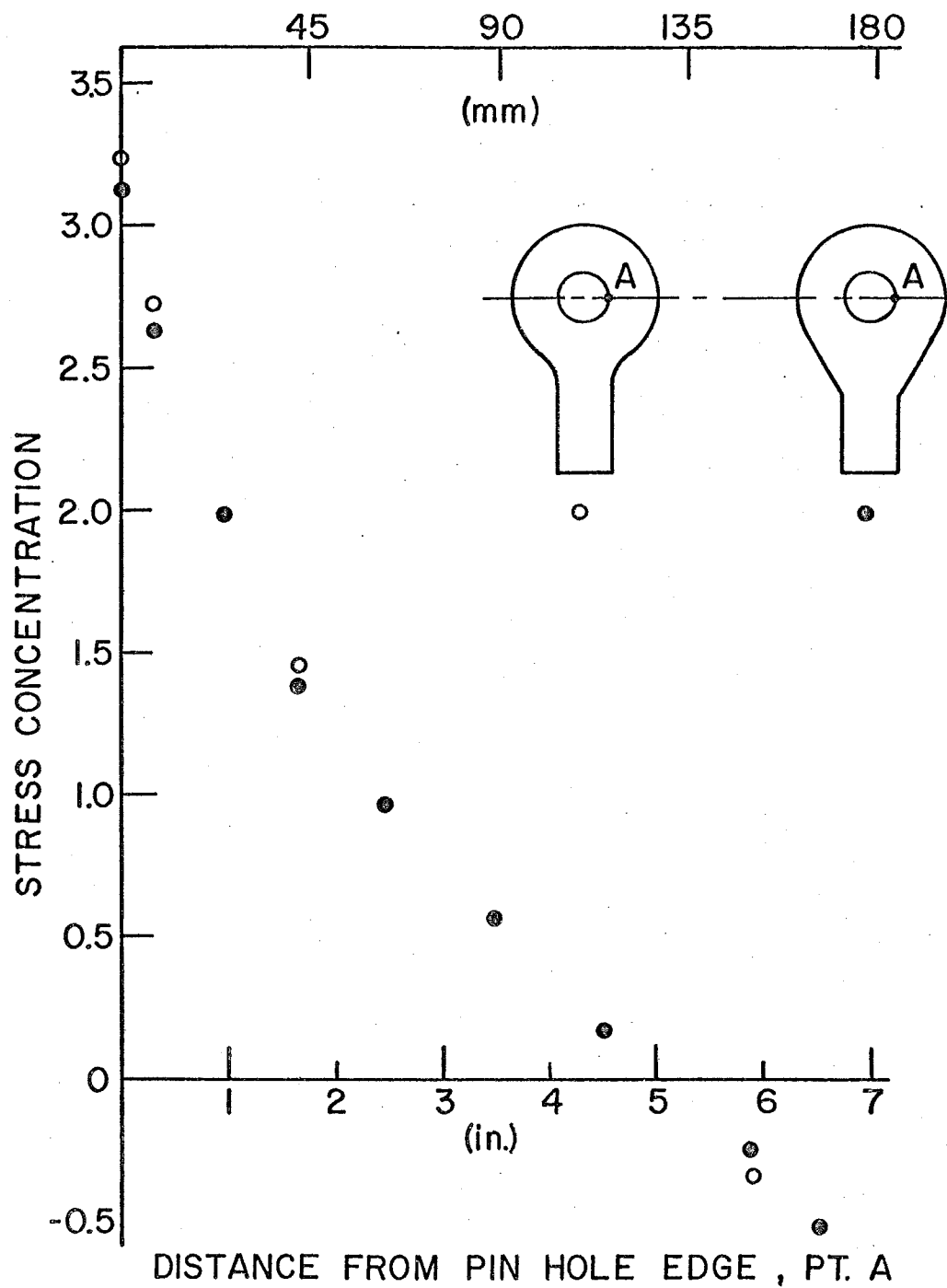
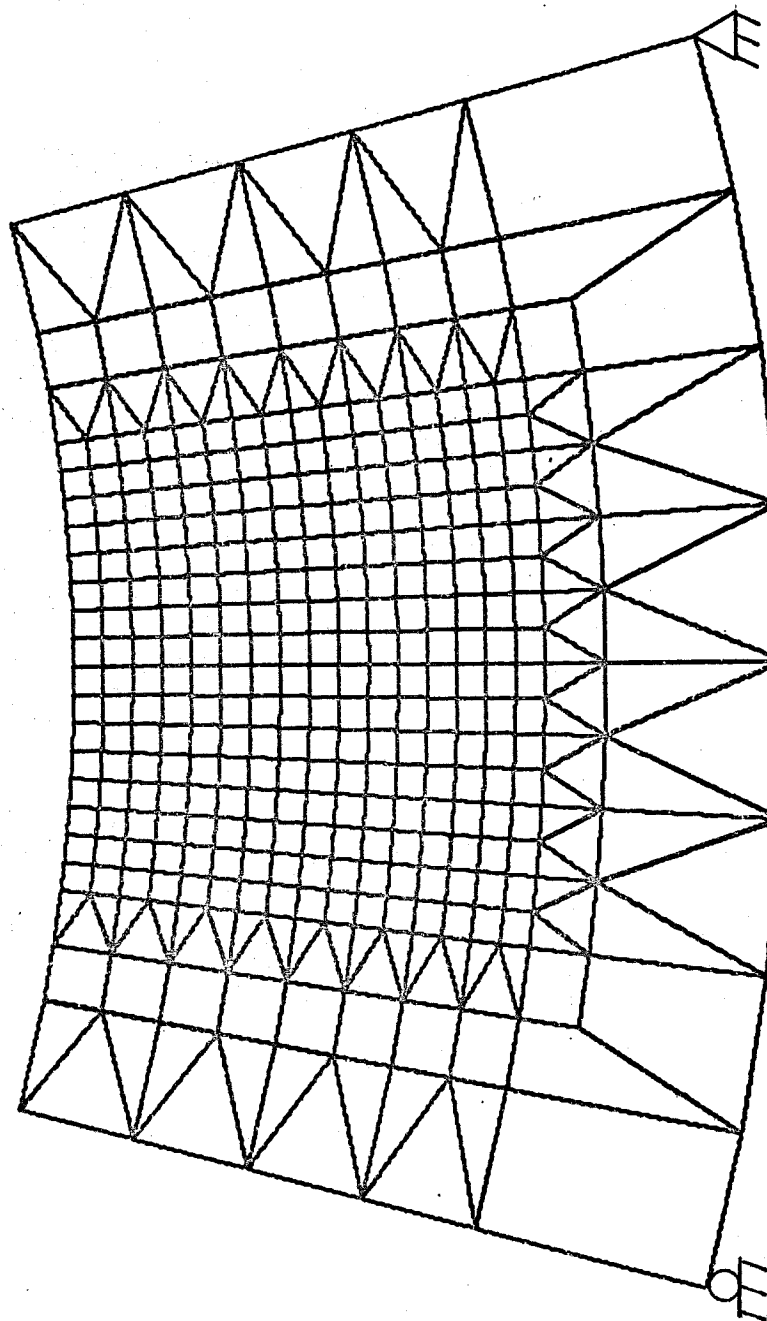


Fig. 20. The Effect of Curved and Straight Line Transition
on the Stress Distribution



375 NODES
388 ELEMENTS

Fig. 21 Discretization and Boundary Conditions of
Substructure for a Fine Mesh Analysis

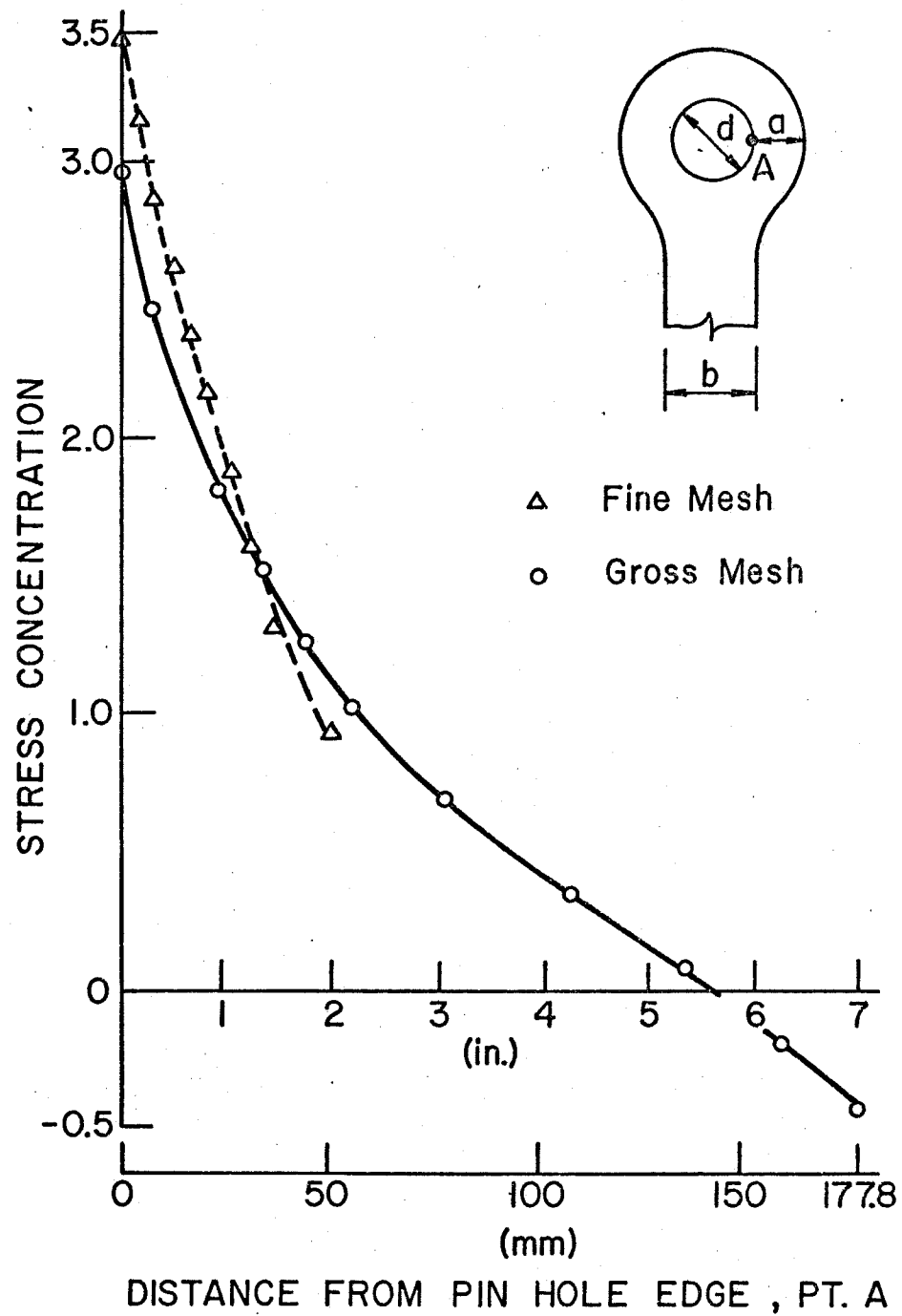


Fig. 22 Effect of Finite Element Size on Stress Distribution

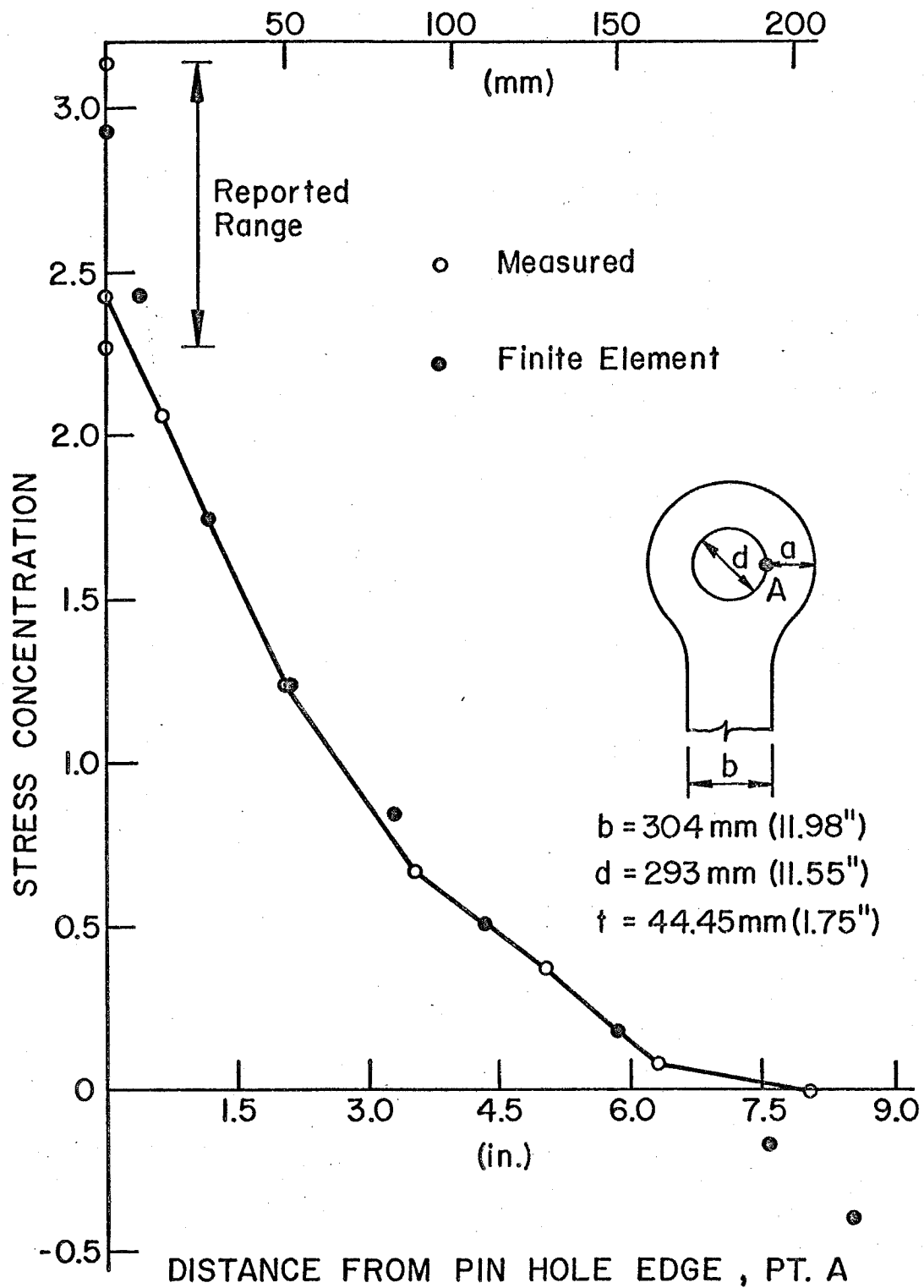


Fig. 23 Comparison of Finite Element Analysis Results and Measured Values

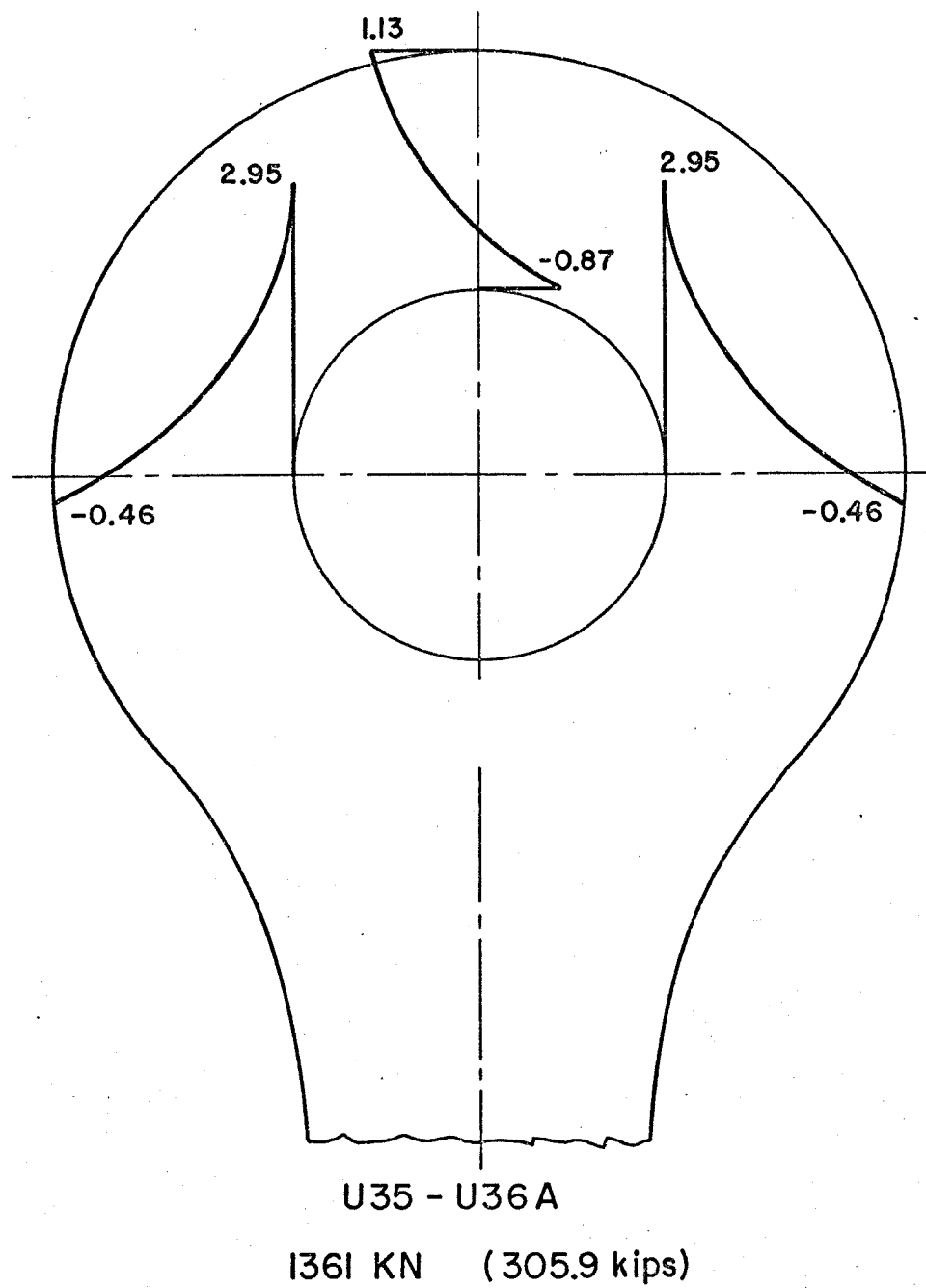
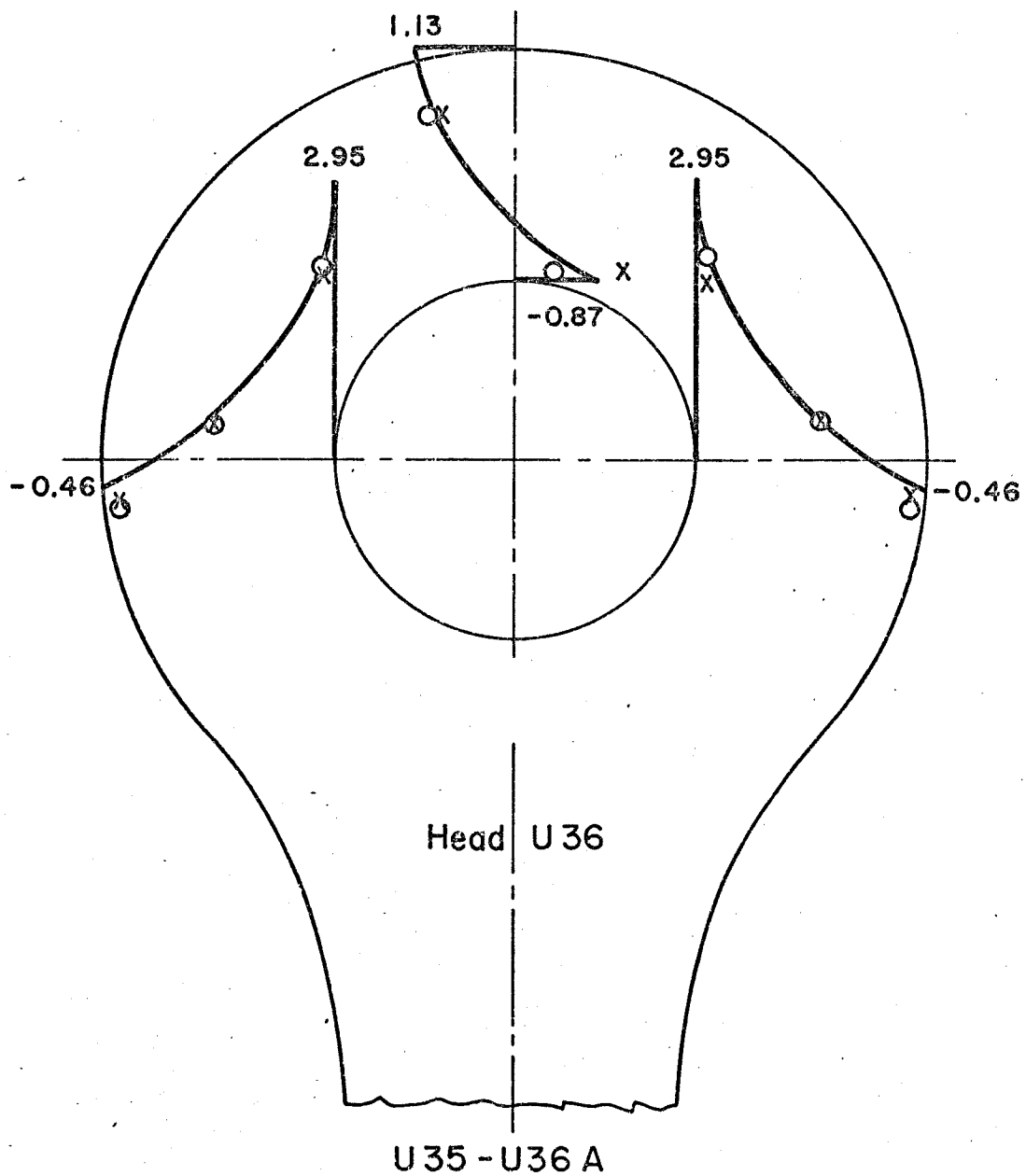


Fig. 24 Results of Gross Mesh Analysis of Eyebar U 35 - U 36
on the Liberty Bridge



x - 1361 kN (305.9 kips)

o - 840 kN (188.9 kips)

Fig. 25 Comparison of Measured and Theoretical Stress
Distributions for U 36A

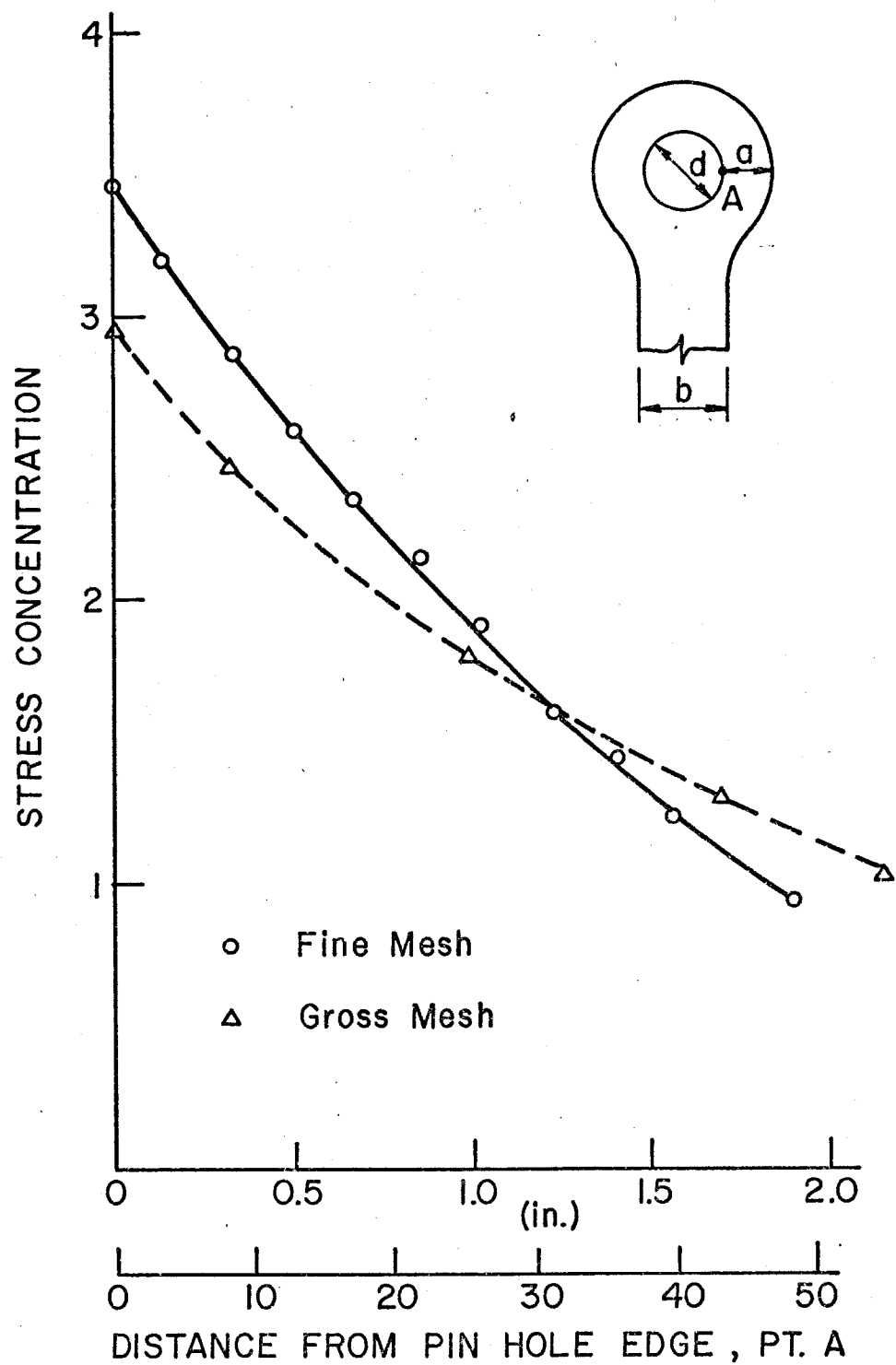


Fig. 26 Enlarged Plot of Gross and Fine Mesh Analysis Results

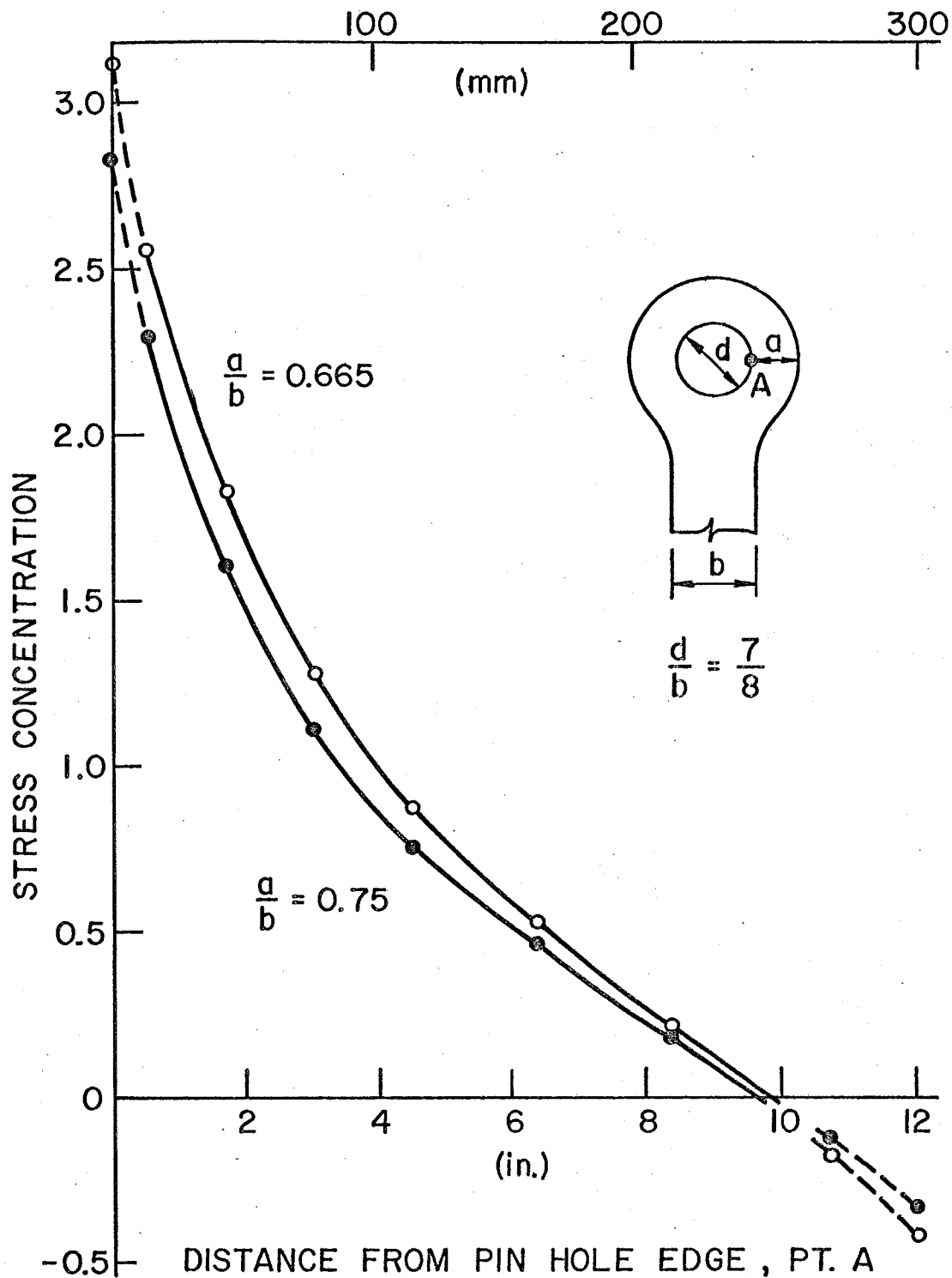


Fig. 27 Stress Distribution for Eyebar Heads with Different Width Ratios, Gross Mesh

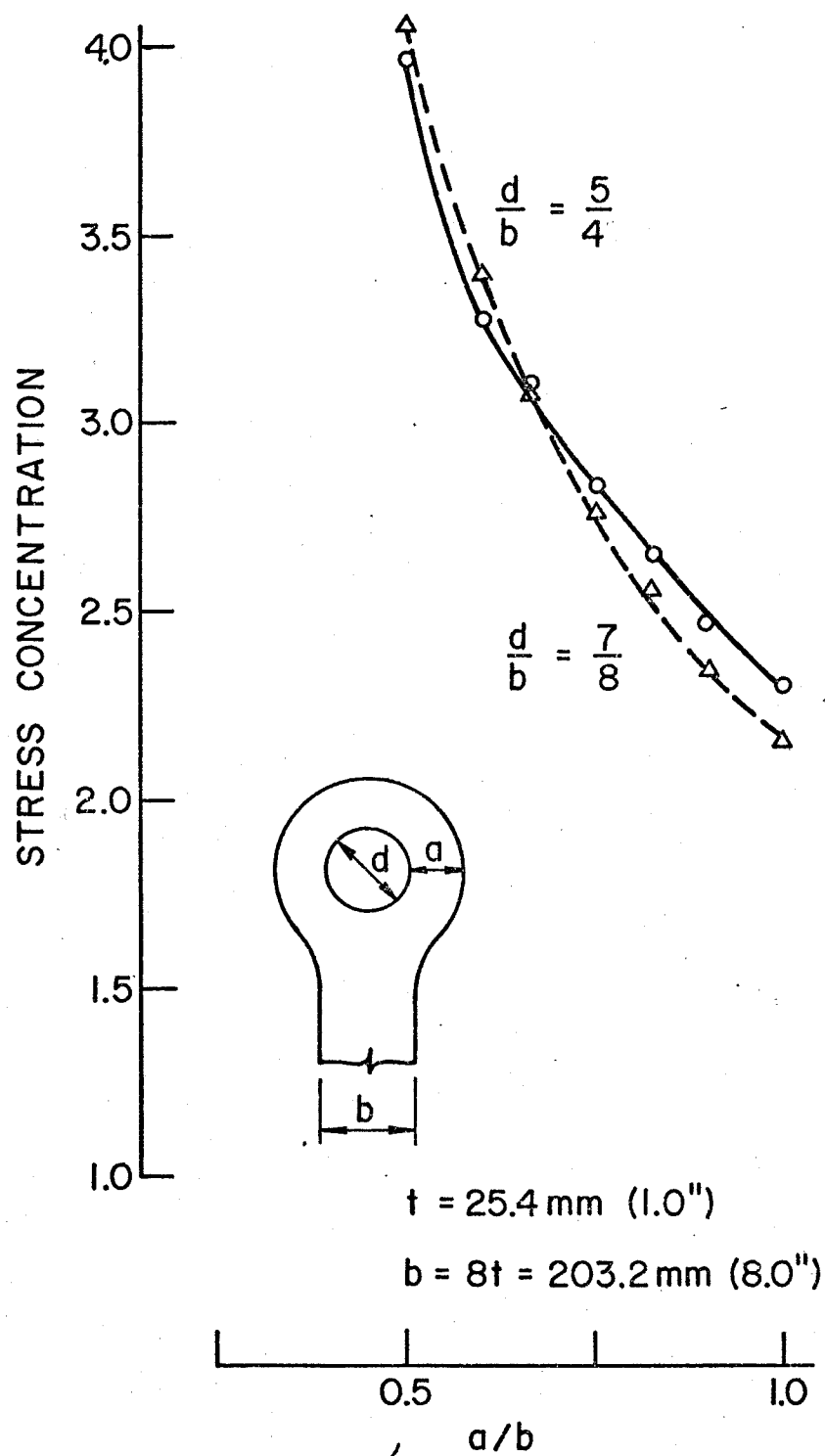


Fig. 28 Effect of Pin Hole Size on the SCF, Gross Mesh

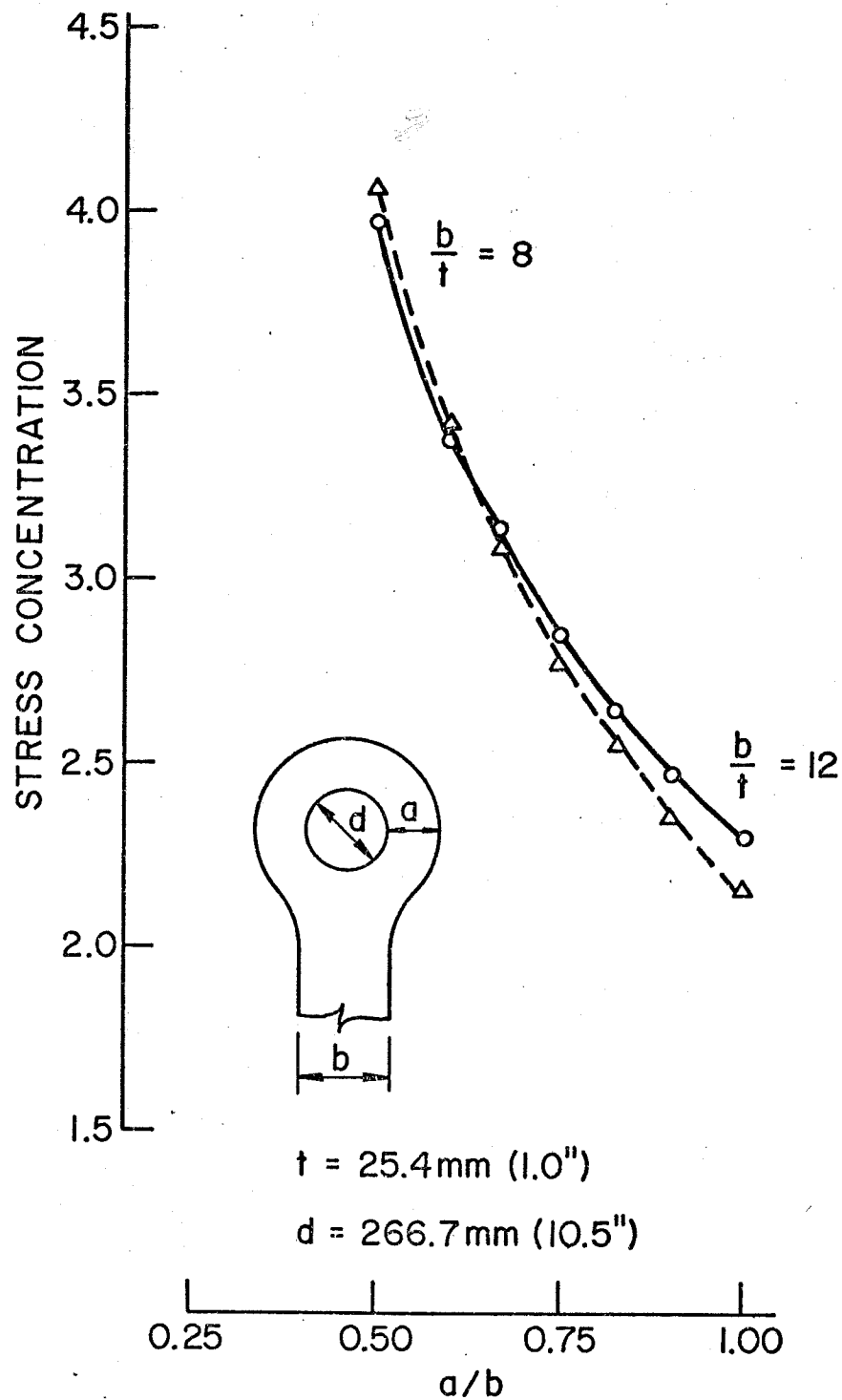
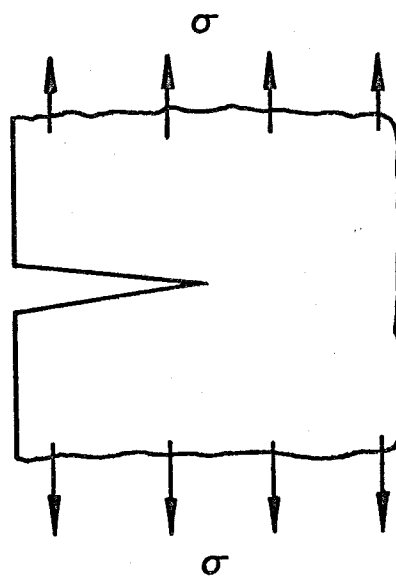
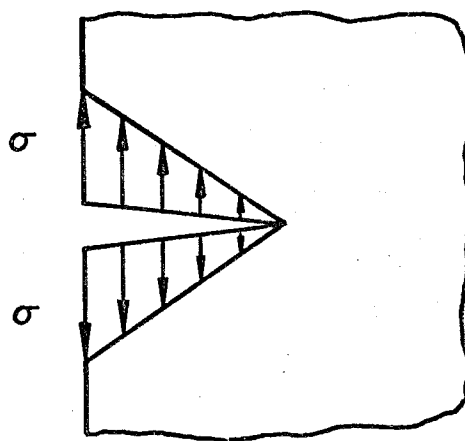


Fig. 29 Effect of Shank Width on the SCF, Gross Mesh



$$F_s = 1.122$$

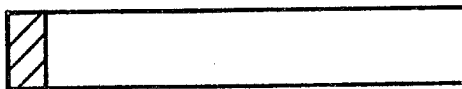


$$F_s = 1.21$$

Fig. 30 Front Free Surface Correction Factor, F_s



$$F_e = 0.6366$$



$$F_e = 1.0$$

Fig. 31 Assumed Crack Shape at Edge of Pin Hole

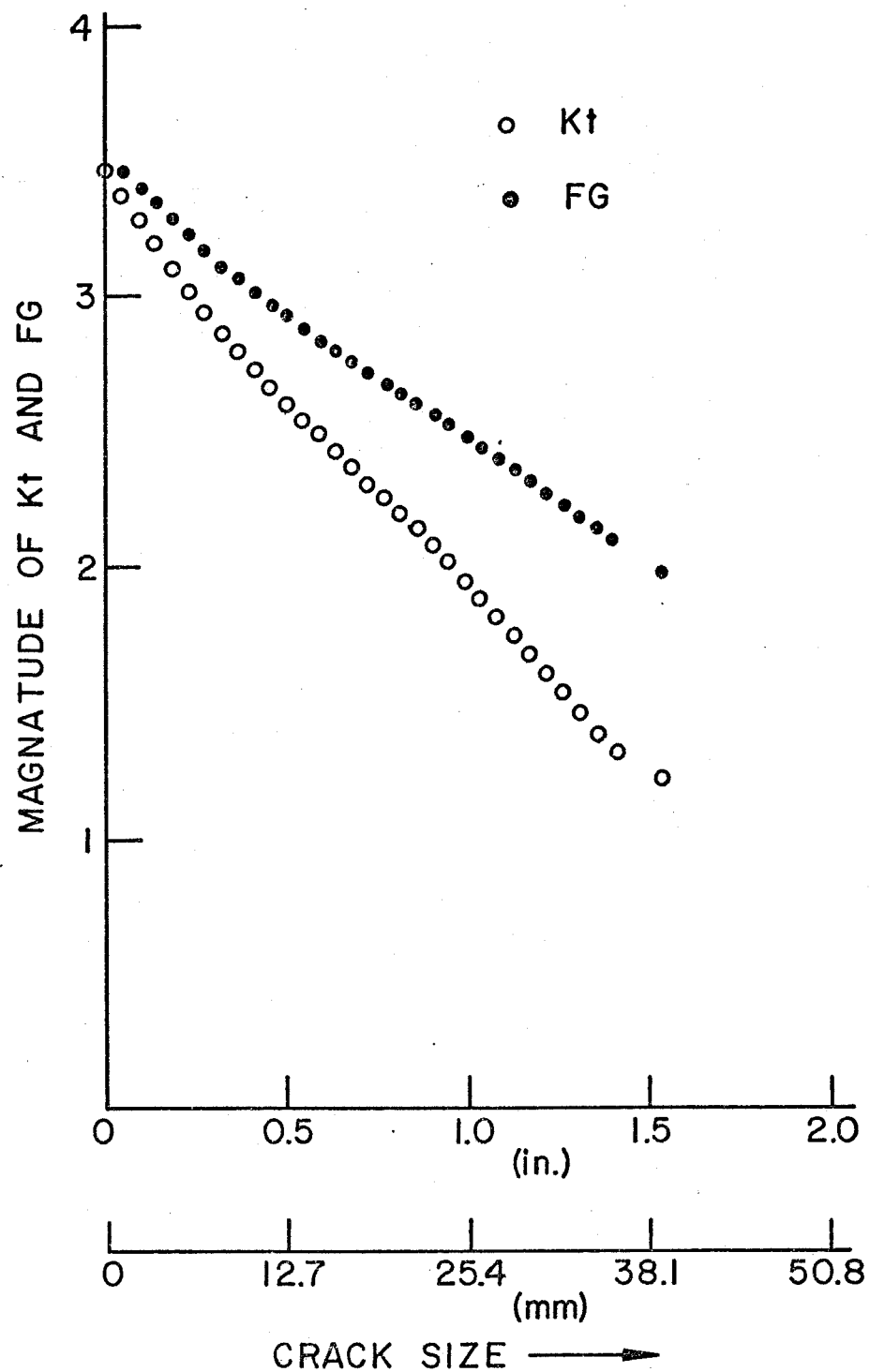


Fig. 32 Stress Concentration Factor K_t and Stress Gradient Correction Factor, F_g as a Function of Crack Size

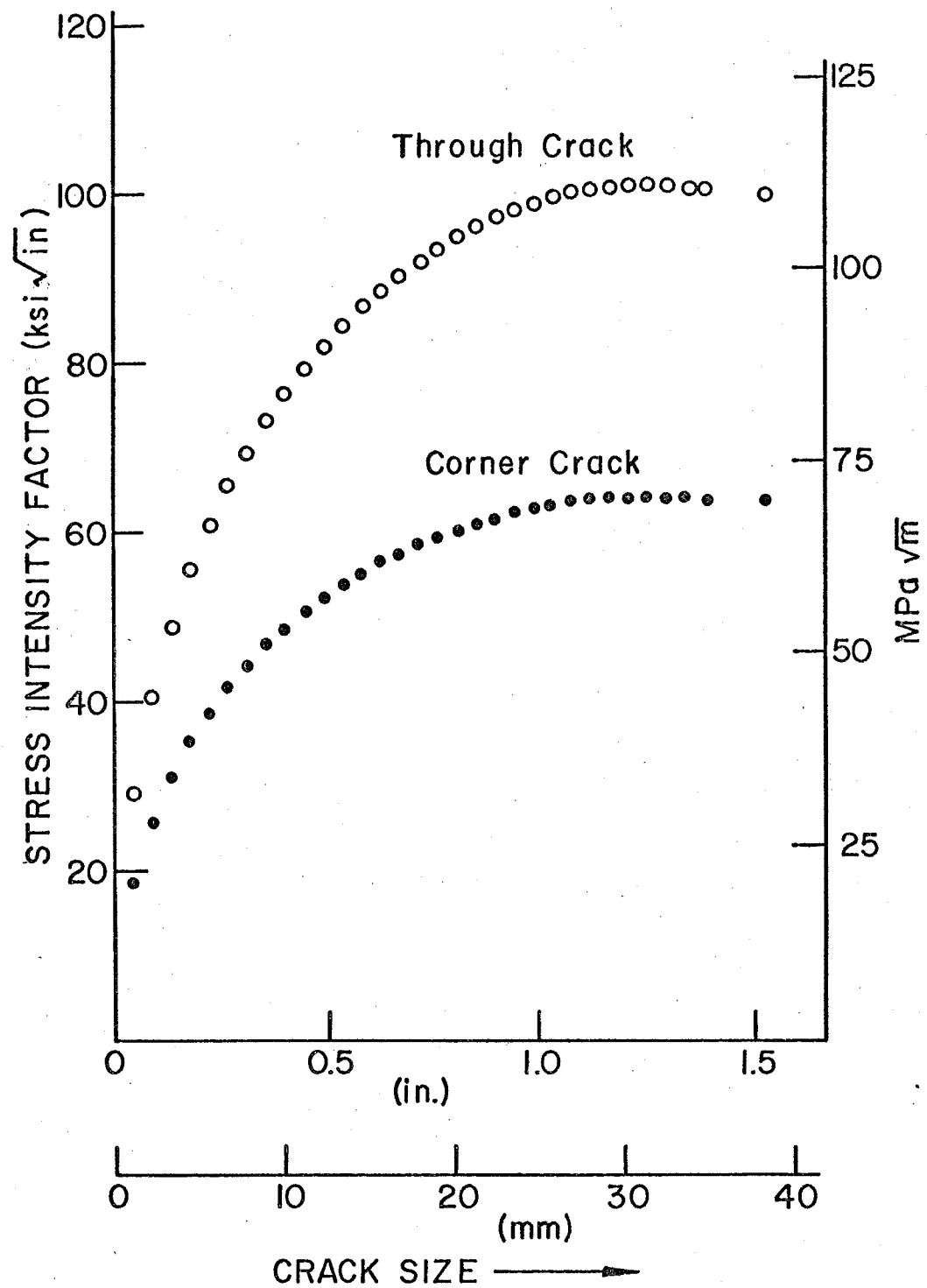
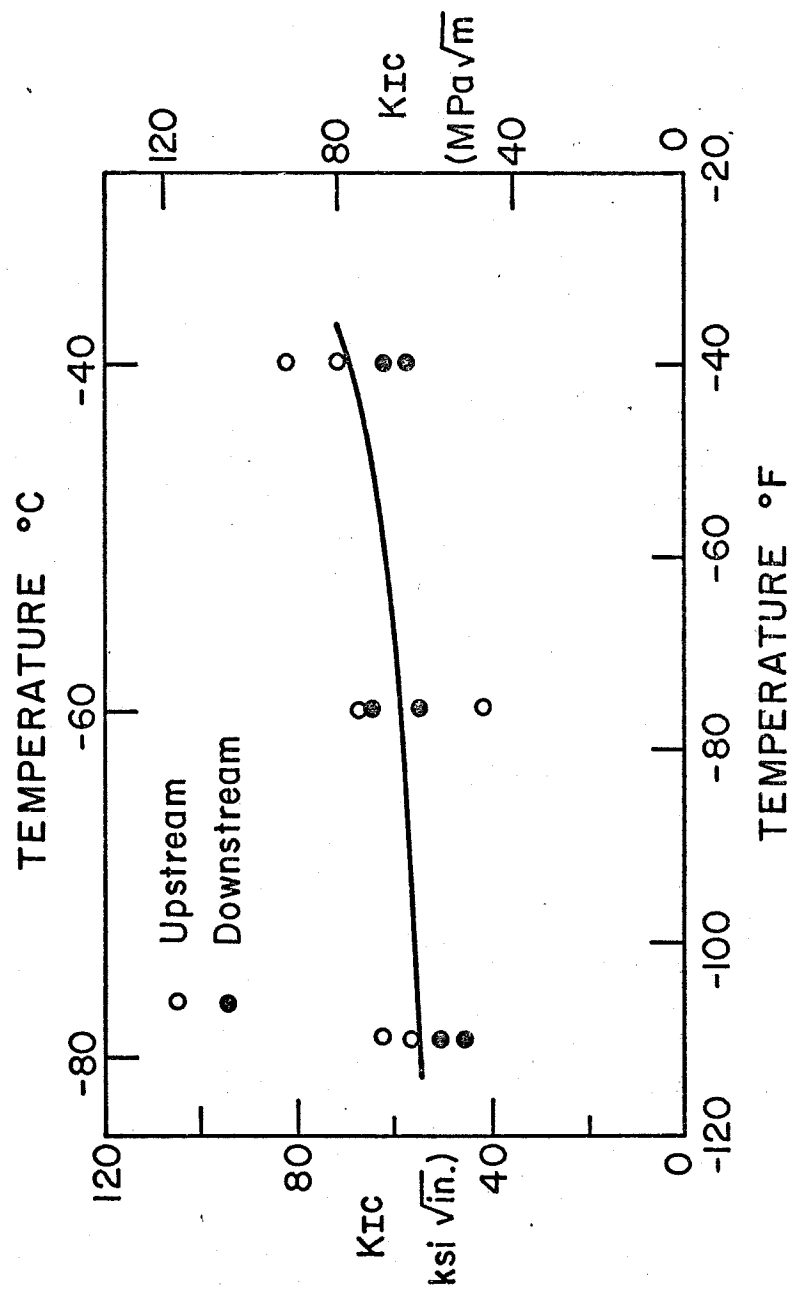


Fig. 33 Stress Intensity Factor as a Function of Crack Size



REFERENCES

1. Steinman, D. B. and Grove, W. G.
THE EYEBAR CABLE SUSPENSION BRIDGE AT FLORIANOPOLIS, BRAZIL,
Transactions of the American Society of Civil Engineers,
Vol. 92, 1928.
2. Steinman, D. B. and Watson, S. R.
BRIDGES AND THEIR BUILDERS, Dover Publications, Inc.,
New York, 1957.
3. National Transportation Safety Board Highway Accident Report,
COLLAPSE OF U. S. 35 HIGHWAY BRIDGE, POINT PLEASANT,
WEST VIRGINIA, Washington, D. C., December 1967.
4. Poletto, R. J.
STRESS DISTRIBUTION IN EYEBARS, M.S. Thesis in Civil
Engineering, Lehigh University, Bethlehem, Pa. 1970.
5. American Institute of Steel Construction,
SPECIFICATION FOR THE DESIGN, FABRICATION AND ERECTION
OF STRUCTURAL STEEL FOR BUILDING, AISC, New York,
New York, 1973.
6. American Association of State Highway Officials
STANDARD SPECIFICATIONS FOR HIGHWAY BRIDGES,
AASHO, Washington, D. C., 1973.
7. American Railway Engineering Association
MANUAL FOR RAILWAY ENGINEERING, Chicago, Illinois, 1973.
8. Blumenfeld, R.
BERECHNUNG VON GEKRUMMTEN STUBEN, Zertsch, Ver
Duetsch-Ing., Vol. 51, 1907.
9. Beke, J.
A STUDY OF STRESSES IN EYEBAR HEADS, Engineering News-
Record, Vol. 87, No. 4, 19
10. Reissner, H. J. and Strauch, F.
RINGPLATTE UND AUGENSTAB, Ingernier Archiv., Vol. 4,
No. 5, 193
11. Timoshenko, S. P. and Goodier, J. N.
THEORY OF ELASTICITY, Third Edition, McGraw-Hill Book Co.,
New York, 1970.

REFERENCES (continued)

12. Fisher, J. W. and Daniels, J. H.
AN INVESTIGATION OF THE ESTIMATED FATIGUE DAMAGE IN MEMBERS
OF THE 380-FT. MAIN SPAN, FRASER RIVER BRIDGE, American
Railway Engineering Association Bulletin No. 688, 1971.
13. Bathe, K. J., Wilson, E. L. and Peterson, F.
SAP IV - A STRUCTURAL ANALYSIS PROGRAM FOR STATIC AND
DYNAMIC RESPONSE OF LINEAR SYSTEMS, Earthquake Engineering
Research Center Report No. EERC 73-11, University of
California, Berkeley, California, June 1973 (Revised
April 1974).
14. Zettlemoyer, N.
STRESS CONCENTRATION AND FATIGUE OF WELDED DETAILS,
Ph.D. Dissertation, Lehigh University, Bethlehem,
Pennsylvania, October 1976.
15. Fisher, J. W., Albrecht, P. A., Yen, B. T., Klingerman, D. J.
and McNamee, B.
FATIGUE STRENGTH OF STEEL BEAM WITH WELDED STIFFENERS AND
ATTACHMENTS, NCHRP Report No. 14, Transportation Research
Board, National Research Council, Washington, D. C., 1974.
16. Fisher, J. W., Pense, A. W. and Roberts, R.
EVALUATIONS OF FRACTURE OF LAFAYETTE STREET BRIDGE,
Journal of the Structural Division, ASCE, Vol. 103, No. ST7,
Proc. Paper 13059, 1977.
17. Hertzberg, R. W.
DEFORMATION AND FRACTURE MECHANICS OF ENGINEERING
MATERIALS, John Wiley and Sons, Inc., New York, N. Y.
1976.
18. Rolfe, S. T. and Barsom, J. M.
FRACTURE AND FATIGUE CONTROL IN STRUCTURES, Prentice-Hall,
Englewood Cliffs, New Jersey, 1977.
19. Tada, H., Paris, P. C. and Irwin, G. R.
THE STRESS ANALYSIS OF CRACKS HANDBOOK, Del Research
Corporation, Hellertown, Pennsylvania, 1973.
20. Tada, H. and Irwin, G. R.
K-VALUE ANALYSIS FOR CRACKS IN BRIDGE STRUCTURES,
Fritz Engineering Laboratory Report No. 399.1, Lehigh
University, Bethlehem, Pennsylvania, June 1975.

REFERENCES (continued)

21. Albrecht, P. and Yamada, K.
RAPID CALCULATION OF STRESS INTENSITY FACTORS, Journal
of the Structural Division, ASCE, Vol. 103, No. ST2,
February 1977.
22. Roberts, R. and Krishna, G. V.
STATIC AND DYNAMIC FRACTURE TOUGHNESS OF EYEBAR MATERIAL
FROM THE CARQUINEZ WEST BRIDGE, Federal Highway
Administration, Draft Copy, 1977.
23. Carter, C. S., Hyatt, M. V. and Cotton, J. E.
STRESS-CORROSION SUSCEPTIBILITY OF HIGHWAY BRIDGE
CONSTRUCTION STEELS, Phase I, Federal Highway
Administration RD-73-3.
24. Paris, P. C.
THE FRACTURE MECHANICS APPROACH TO FATIGUE, Fatigue--An
Interdisciplinary Approach, Proc. of the Tenth Sagamore
Army Materials Research Conference, Syracuse University
Press, 1964.
25. Hirt, M. A. and Fisher, J. W.
FATIGUE CRACK GROWTH IN WELDED BEAMS, Journal of
Engineering, Fracture Mechanics, Vol. 5, 1973.
26. Barsom, J. M.
FATIGUE CRACK PROPAGATION IN STEEL OF VARIOUS YIELD
STRENGTHS, Applied Research Laboratory, United States
Steel Corporation, 1971.
27. Paris, P. C.
TESTING FOR VERY SLOW GROWTH OF FATIGUE CRACKS,
Closed Loop, MTS System Corporation, Vol. 2, No. 5,
1970.
28. Crooker, T. W. and Lange, E. A.
HOW YIELD STRENGTH AND FRACTURE TOUGHNESS CONSIDERATIONS
CAN INFLUENCE FATIGUE DESIGN PROCEDURES FOR STRUCTURAL
STEELS, Welding Research Supplement, Vol. 49, No. 10,
1970.
29. Batchler, B. P.
THE FATIGUE STRENGTH OF DISCONTINUOUS BACKUP BAR DETAILS,
M.S. Thesis, Lehigh University, Bethlehem, Pennsylvania,
October 1977.

VITA

The author was born in New Bedford, Massachusetts on January 21, 1950. His primary and secondary education was received in the New Bedford School system. In July of 1967 the author joined the United States Marine Corps and was assigned to an Engineer Battalion. He received training to operate forklifts, cranes, bulldozers, graders and other types of earth moving equipment. He was involved in the building of ammunition depots and the regular maintenance of roads in Camp Lejune, North Carolina. While most of the tour of duty was spent in the United States, 4 months were spent in the Caribbean and 15 months on Okinawa. The author completed his tour of active duty as a Corporal E-4, and was Honorably Discharged in September 1970.

In September of 1972 the author entered Bristol Community College in Fall River, Ma. and received an Associate of Engineering Degree with Honors in May of 1974 at which time he started study at Southeastern Massachusetts University, North Dartmouth, Ma. He was awarded a Bachelor of Science in Civil Engineering degree with Distinction in June 1976.

In September 1976 the author entered Lehigh University as a half-time research assistant in Fritz Engineering Laboratory in the Fatigue and Fracture Division. Since that time he has worked on "Stress History Measurements on the Glenfield Bridge" and "Fatigue and Fracture Resistance of Eyebars on the Liberty Bridge" with the latter project forming the basis of this thesis.